DESIGN AND MODELING OF HIGH TEMPERATURE, HIGH HEAT FLUX TEST APPARATUS USING LIQUID IMMERSION

Thesis

Submitted to

The School of Engineering of the

UNIVERSITY OF DAYTON

in Partial Fulfillment of the Requirements for

The Degree

Master of Science in Chemical Engineering

by

George Robert Doyle III

UNIVERSITY OF DAYTON

Dayton, Ohio

December, 2003

DESIGN AND MODELING OF HIGH TEMPERATURE, HIGH HEAT FLUX TEST APPARATUS USING LIQUID IMMERSION

APPROVED BY:

ABSTRACT

DESIGN AND MODELING OF HIGH TEMPERATURE, HIGH HEAT FLUX TEST APPARATUS USING LIQUID IMMERSION

George R. Doyle III
University of Dayton, December 2003

Advisor: John L. Graham

Hydrocarbon fuels have been the focus of U.S. Air Force propulsion research for many years. Recently, they are concerned with the highly stressed behavior of fuels during their application in regenerative heating processes within rocket engines. This thesis discusses the design and performance of a liquid-solid heat transfer apparatus that will be used to deliver heat to fuels. The apparatus uses a eutectic drawsalt mixture which operates between 260°C and 565°C. Experimentation yielded the highest heat flux to be 1.645 Btu/in^{2}s at 468°C at steady state water flowrate of 0.435 L/min (18.8 ft/s). A model, based on energy balances over finite volume elements, was used to predict the heat flux for the apparatus. The heat transfer coefficients were the most difficult aspect of the model and were predicted using standard correlations for Nusselt numbers. The general trend of the experimental results was matched by the model. The model predicted under the same conditions as the peak experimental heat flux to be 1.373 Btu/in^{2}s and a temperature change of 48.1°C. Future experiments are planned using different salt mixtures, test fluids, and configurations.

ACKNOWLEDGEMENTS

Special thanks to my research advisor John Graham and the Air Force Principal Investigator Richard Wills for giving me the opportunity to work on this project, their patience, and their direction in completing this thesis.

I would also like to express thanks to Dr. K. J. Myers for his help over the past few years with classes and research opportunities and to Dr. S. S. Sandhu for helping with my thesis by serving on my committee. Also, I would like to sincerely thank my parents, Dr. George Doyle, Jr. and Patricia Doyle, for their support, especially these past few years. Finally, I would like to thank Anish Desai and Jesse Contreras for their help in applying class work to this thesis.

TABLE OF CONTENTS

APPENDICIES

LIST OF ILLUSTRATIONS

LIST OF TABLES

LIST OF SYMBOLS & ABBREVIATIONS

Abbreviation:	Description:
AFRL	United States Air Force Research Laboratories
EDM	eutectic drawsalt mixture
HTS	heat transfer salt
ID	inner diameter
LOX	liquid oxygen
Nu	Nusselt number
OD	outer diameter
PDE	partial differential equation
Pr	Prandtl number
Re	Reynolds number
USAF	United States Air Force
WPAFB	Wright Patterson Air Force Base

Symbol:	Description:
A_0	heat transfer area (m^2)
C_p	molar specific heat capacity (J/mol-K)
C_p	specific heat capacity (J/kg-°C)
D	diameter, D_0 inner diameter, D_1 outer diameter (m)
G	mass velocity (kg/m^2-s)
h	heat transfer coefficient (W/m^2-K)
H	enthalpy, H_0 reference enthalpy, H_1 inlet enthalpy, H_2 outlet enthalpy, H_i enthalpy of a given material (J/mol)
k	thermal conductivity (W/m-K)
$\dot{m}$	mass flow rate (kg/s)
n	moles
$\dot{n}$	molar flow rate (mol/s)
N	impeller speed (rpm)
Q	heat (J)
$\dot{Q}$	heat flow (J/s)
$\dot{q}$	heat flux (W/m^2 or Btu/in^2-s)
r	radius, r_0 inner radius, r_1 outer radius, r_2 salt layer radius (m)
T	temperature, T_m melting temperature, T_0 reference temperature, T_1 inlet temperature, T_2 outlet temperature (°C)

t	time (s)
U	total internal energy (J)
v_z	time averaged fluid velocity (m/s)
v_θ	tangential velocity (m/s)
W	work (J)
ΔH_{vap}	heat of vaporization (J/kg)
b	Bessel function constant of integration
ϕ	viscosity ratio
μ	viscosity, μ_b, viscosity of bulk fluid, μ_0, viscosity at the wall (kg/m-s)

CHAPTER I

INTRODUCTION

Material compatibility is essential in any machine, building, or product, especially under operating conditions. To avoid failure, interactions between materials should be understood before they are used together. This search for understanding drives the research of material compatibility under high stresses, including high heat flux.

High heat flux conditions often occur in rocket propulsion systems. The beginning of liquid fueled rockets was the theories developed by the Russian, Konstantin Tsiolkovsky, who first described rocketry in 1883. However, Robert Goddard was the first to actually build a liquid propelled rocket engine. At first Goddard experimented with solid rocket fuels and then went on to explore liquid propellants. In 1926, Goddard tested the first liquid propelled rocket, flying to 41 feet. Amateur rocket societies in Russia, Germany and the United States developed during the 1920s and 1930s and were eventually incorporated into military research groups [1]. One particular member of the American Interplanetary Society (later renamed to the American Rocket Society) was James Wyld. He developed the idea of regenerative cooling, which circulates fuel around the combustion chamber to cool the engine and to heat the fuel prior to burning. While his first attempt in a regenerative engine failed, later tests

proved his designs valid. These designs are now the basis for all modern liquid propelled rockets [2].

Two examples of these regenerative rocket engines are the Saturn V F-1 and the XLR99 rocket engines. Both of these engines used liquid propellants and were equipped with extensive cooling to prevent high temperature damage [3, 4].

The F-1 rocket engine, used to propel the Apollo space modules into orbit, is an example of high temperature heat flux coolant systems. This particular rocket used RP-1 (a hydrocarbon fuel which is derived from kerosene) as a cooling fluid around the combustion chamber and venturi nozzle. After cooling the engine components, the RP-1 was fed into the combustion chamber, along with liquid oxygen (LOX). The combustion chamber was machined with tubular walls to facilitate cooling of the chamber and preheating of the fuel as developed by Wyld. An important aspect of the F-1 and particularly of RP-1/LOX propulsion was that it exhibited heat flux around 7 Btu/in^2s [3, 5].

The X-15A research rocket, which used the XLR99 engine, is another example of a high heat flux engine. Launched from a USAF B-52 bomber, the X-15A was designed to provide inflight data on aerodynamics, structural integrity, flight controls, and physiological effects of high altitude, high speed flight. The XLR99 throttleable engine was capable of producing up to 60,000 lbs of thrust. While its fuel was anhydrous ammonia rather than hydrocarbons, it also used a fuel-based coolant system to prevent high heat stress effects on the engine. The coolant system used ammonia fuel to extract heat from the venturi style nozzle,

and the ignition chamber, which were constructed from welded, wire-wound tubes [4].

Both of these rocket engines used tube walled combustion chambers, and it is these types of combustion chambers that are being simulated by a heat flux apparatus. While, the XLR99 engine used an ammonia based propellant, the general design is still applicable. Hydrocarbons, on the other hand, as fuels and coolants have been an integral part of United States Air Force (USAF) propulsion for several good reasons. One important advantage of hydrocarbon fuels is that they are readily available and easily synthesized, unlike liquid hydrogen or anhydrous ammonia, which are costly to manufacture because of refrigeration processing. Also, hydrocarbon fuels are easily stored and handled, and their properties can be changed through additives. Avgas, which is a hydrocarbon fuel used in aviation piston engines, usually is stable up to one year after manufacturing [5].

However, there are some disadvantages to using hydrocarbon fuels. Often hydrocarbons exhibit instability when exposed to high temperatures. Decomposition products, such as carbon deposits, can adversely affect the fuel system. The first such product consists of peroxides, which remain dissolved in the fuel. Peroxides have the potential of attacking elastomers that serve as major components or seals in the engine. Further decomposition reactions produce gums and particles, which may form deposits and clog fuel lines. Other changes that occur during storage are oxidation to more reactive hydrocarbons and evaporation of the more volatile components [5]. With regard to their

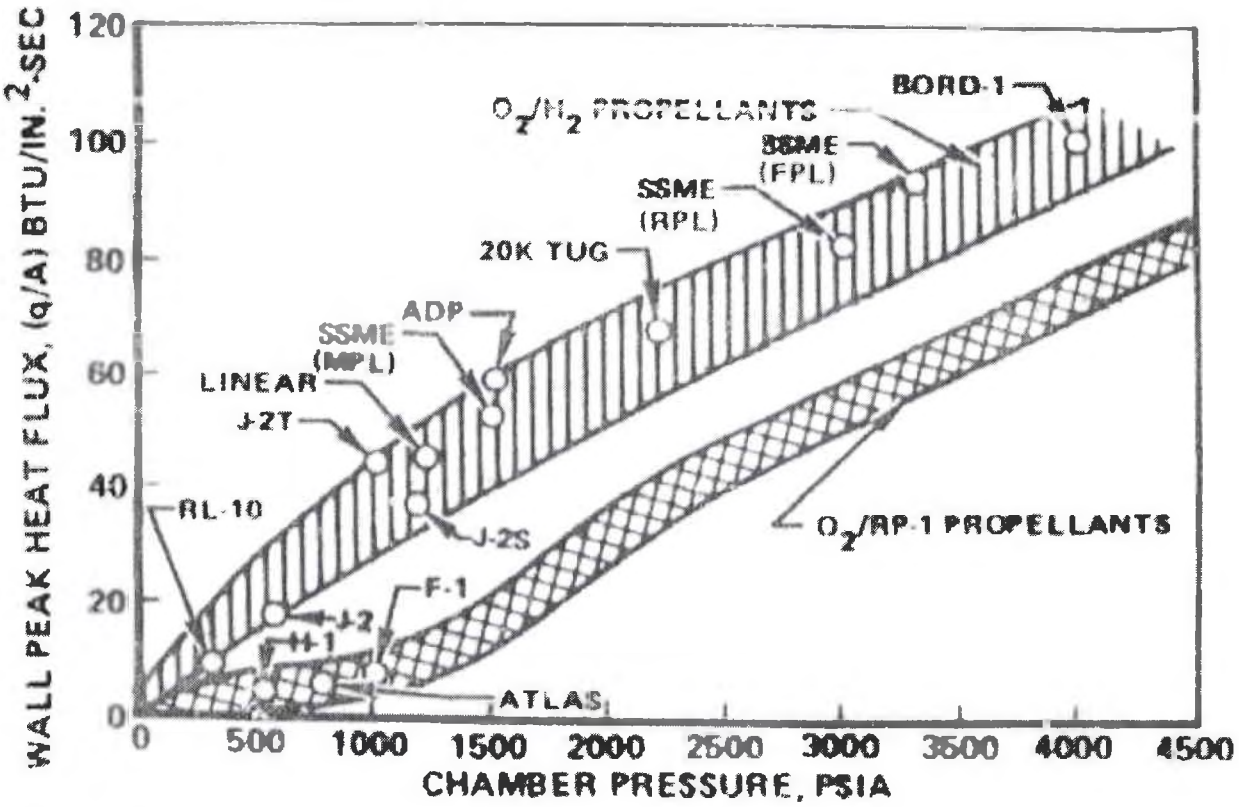

Figure 1: Flux of Propellant Combinations Used in Modern Rockets. Wagner, Shoji [6].

behavior within the combustion chamber, decomposition products may influence the amount of heat flux absorbed by the coolant fuel. A low mixture ratio of oxidizer to fuel results in deposition of a carbon layer on the chamber walls. This carbon layer provides resistance to heat flow, which actually promotes the lifetime of the engine. Despite this insulation layer, modern hydrocarbon rockets are projected to produce heat fluxes up to 80 Btu/in^{2}s [6].

A comparison of various propellant systems based on heat flux as a function of chamber pressure shows why rockets using hydrocarbons fuels are still a concern. Such a comparison comes from Wagner and Shoji and is given in

Figure 1 [6]. As can be seen in Figure 1, the F-1 engine ranks fairly low with regard to combustion chamber heat flux, which is probably due to the low chamber pressure. Modern hydrocarbon propellants fall into the range indicated by "O_2/RP-1 PROPELLANTS," and these have a much higher chamber pressure, which results in more thrust and higher heat flux. Overall, modern rockets have a maximum heat flux around 115 Btu/in^{2}s within the combustion chamber cooling jacket [6].

As stated before, the combustion chamber is cooled by fuel prior to entering the combustion chamber, which is known as regenerative cooling. Regenerative cooling is a common method of preheating a fuel and requires less energy via ignition [7]. High fuel flowrates within the heat exchangers are required such that the rate of heat extraction is great enough to prevent high heat damage to the combustion chamber. Damage that most frequently occurs is due to high temperature creep and low-cycle fatigue [8]. These high temperature effects are the reasoning behind why rocket engines must be cooled with high flow rates of fuel up to 600 ft/s [6].

The objective of this project is to design and model a test rig that can expose model test fluids (such as water) to high heat fluxes at high temperatures. Important information that will result from this study includes a working model that can predict the behavior of liquid-solid-liquid heat exchange and validation of that model with a working apparatus. Particularly, US Air Force research is concerned with the highly stressed behavior of fuels during their application in regenerative heating processes within rocket engines. Ultimately, a test rig that

can supply a heat flux up to 115 Btu/in^{2}s will be developed, from which behavior of test fluids and test pieces can be established.

CHAPTER II

BACKGROUND

Heat Flux Apparatuses

The design of high temperature high heat flux test apparatuses used in this project were chosen to take one of four configurations: 1) direct resistance heating, 2) high pressure combustion, 3) direct radiation heating, and 4) liquid immersion heating. Also, there are other rocket apparatuses in development at the NASA Glenn Research Center.

Direct Resistance Heating

The application of high amperage current through a test piece to deliver thermal energy to a test fluid was built for direct resistance heating. With high enough current running through a test piece, its electrical resistance will generate heat which is transferred to the flowing test fluid. The temperature change of the test fluid is measured to determine the delivered heat flux. Also, any interactions or decompositions between the test piece and the fluid are observed. Figure 2 shows a schematic of the direct resistance heater. The major limiting factor of this test rig is how much heat the test piece can produce via conversion of electrical energy to thermal energy. The main resistance to heat transfer is the thermal boundary layer between the test fluid and the test piece. However, direct resistance heating is

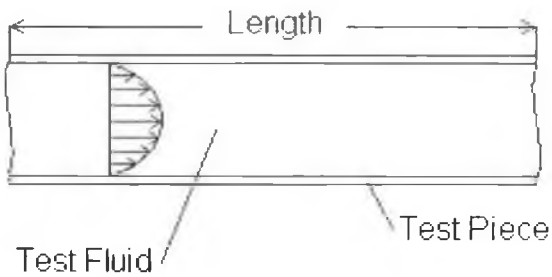

Figure 2: Schematic of Direct Resistance Heater.

viable because of its ease of operation and its ability to apply heat flux to the test fluid.

High Pressure Combustion

A burner exploiting the combustion of propane and oxygen to deliver heat flux through a gas-solid interface has been developed. The combustion of hydrocarbons produces adiabatic flame temperatures over 2,000°C [7]. Combustion takes place within the ignition chamber and the hot product gases flow over the test piece. Heat transfer in this case is limited by a gas-solid boundary layer around the test piece. However, with a high temperature flame at a high gas velocity, this boundary layer is greatly reduced. Another advantage of this apparatus is that it is similar in configuration to an actual rocket engine, and thus, more closely simulates the real world configuration. This second configuration, known as the burner rig, is currently under research at the Air Force Research Laboratories (AFRL) at Wright Patterson Air Force Base (WPAFB). It has undergone several stages in design, and will be further developed until ready for research on modern fuels. Results so far have

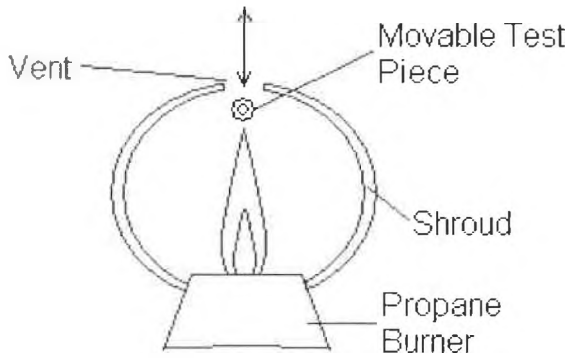

Figure 3: Burner Schematic.

reached up to 0.52 Btu/in^{2}s and it is estimated to be able to reach 20 Btu/in^{2}s in future designs [9]. Figure 3 shows a general schematic of the burner apparatus.

Indirect Radiation Heating

The third configuration concentrates high energy light onto the test piece. It operates by focusing light from a water cooled arc lamp, producing up to 300kW for a five minute period. A mirror configuration then focuses that light via reflection onto the test piece to deliver the energy. Limiting factors in this configuration include the efficiency of heat transfer via radiation to conduction

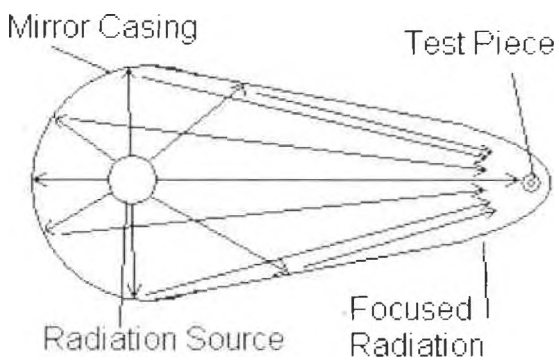

Figure 4: Radiation Heater Schematic.

through the test piece. Use of this heat flux apparatus has not been fully exploited, but a heat flux up to 14 Btu/in^{2}s has been reported [9]. Figure 4 shows a schematic of the arc lamp with test piece.

Liquid Immersion Heating

The final configuration, the liquid immersion heat exchanger, is the focus of this thesis. It takes advantage of the higher heat transfer rates encountered at a liquid-solid interface than for gas-solid boundary layers. In comparison to the burner method, higher heat transfer rates occur because the density of the liquid is greater than the combustion gases. Also, with adequate mixing any boundary layer effects may be reduced to allow greater heat transfer. Thus, using this configuration, heat transfer is limited by conduction and convection. Another advantage that the immersion heater possesses is that the immersion bath functions as a large heat reservoir. This implies that a significant heat withdrawal by the test fluid does not reduce the temperature of the bath significantly. Especially for a well mixed liquid, this is essential since the tests were run at steady state conditions. Another advantage to the liquid immersion heater is that it does not require fuel and oxidizer to operate. The heating material is not being consumed and so it lacks the extra operational costs of the burner.

NASA Glenn Rockets

There are two other configurations under research at the NASA Glenn Research Center. The first of these is a rocket engine fueled by a metallized gelled liquid propellant. This configuration is testing the gelled propellant which is metallized with aluminum. The peak heat flux occurred at the nozzle and

reached a value of 6.5 MW/m^2 or 3.975 Btu/in^2s [10]. The second design also uses a rocket engine to provide the heat flux to water cooled panels. Running at chamber pressures from 130 to 520 psia and mixture ratios from 1.5 to 5.0 of oxidizer to fuel, the rocket reached a maximum heat flux of 8.8 Btu/in^2s [11]. These heat flux results show that further development is required to deliver the goal of 115 Btu/in^2s.

Liquid-Solid Immersion Heat Flux Apparatus

The focus of this thesis is the liquid-solid immersion heat flux apparatus. The immersion bath can be any liquid. However, certain thermal properties, such as thermal conductivity, heat capacity, volatility, and stability, are essential to obtain high heat flux. Thermal conductivity is a material property that describes how fast a material conducts energy in the form of heat. Hence, the immersion bath should have a high thermal conductivity to maximize heat flux. Heat capacity is the amount of energy required to raise the temperature one degree for a given amount of a substance. A high heat capacity implies that it takes large amounts of energy to change the temperature of a given amount of substance. Thus, to ensure steady state operation, a high heat capacity fluid should be used. The volatility of the liquid should be low. This will ensure that the liquid does not evaporate below its boiling point, which would reduce maximum operating temperature of the apparatus. Thermal stability is also imperative to ensure that reaction products neither evolve from the liquid bath nor that they interact with the test piece. In addition to these qualities, it should be

non-corrosive to most metals, since the cooling jackets are primarily made from steels. Finally, it should be non-toxic at high operation temperatures.

One group of substances that fits this description is molten salts. Mixtures of various inorganic salts, when melted, have a wide range of operational temperatures, excellent thermal properties, and the ability to store large amounts of thermal energy. There are two major kinds of molten salts that have been used extensively since the 1930s: heat transfer salt (HTS) and drawsalt. HTS is a mixture of potassium nitrate, sodium nitrate and sodium nitrite in a 53/7/40 weight percent ratio, respectively. Melting at 142°C, HTS has an operation range up to 482°C. Drawsalt is a 60/40 by weight mix of sodium nitrate and potassium nitrate. Particularly, the eutectic drawsalt mixture (EDM), 46/54 ratio of sodium nitrate to potassium nitrate, was used as the immersion bath in this project. Its operational temperature range is from about 250°C to 565°C. Above 565°C the drawsalt begins to decompose, producing toxic NO_x. The major reason for using EDM is that its thermal stability is greater than that of HTS and some other heat transfer salt mixtures. Other salts tend to decompose into hazardous gasses, such as NO_2 for HTS, and thus require more equipment, such as an inert atmosphere, to maintain the stability. Also, EDM has a broader operating temperature range, which will yield a higher heat flux [12].

CHAPTER III

EXPERIMENTAL METHODS

The initial experiment consisted of testing the heat transfer properties of a gas-solid interface. This experimental set up used a copper and stainless steel test piece through a 12" tube heater (Lindberg 55035A) where the heat transfer fluid was air. The copper test piece was standard quarter inch refrigeration tubing (Cole-Parmer A-34671-10), while the stainless steel test piece was a thin walled $1/16^{th}$ inch tube with a 0.050" inner diameter (Alltech 3004). These experiments were performed as a prelude to liquid-solid heat transfer.

The liquid immersion heat exchanger experiments used several different configurations. Initially, a water bath was used to test low temperature conduction and convection. Next, a conduction tube applying both water and the eutectic drawsalt mixture (EDM) was used. Finally, taking advantage of higher heat transfer coefficients, a large stirred bath with the EDM and water was the final configuration. The overall goal is to apply the molten EDM in a heat flux apparatus to test the properties of future fuels. Water was used in addition to the EDM because their rheological and thermal properties are similar at their operating temperatures as shown in Appendix B.

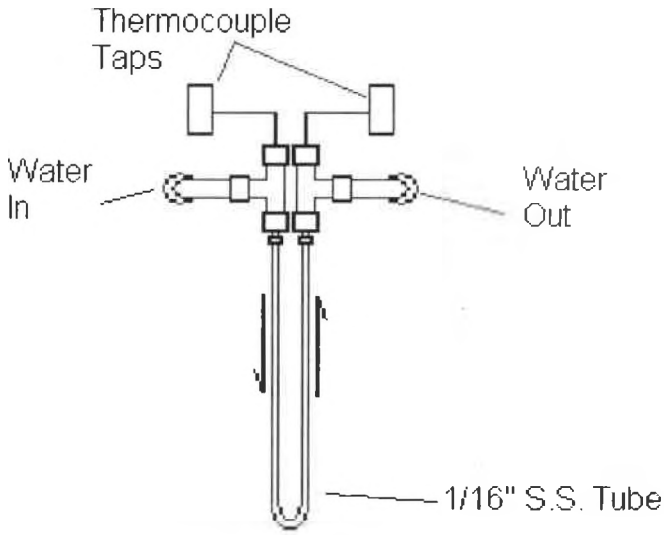

Figure 5: Bulkhead Schematic with Test Piece.

Each of these configurations had a common piping bulkhead to which the test piece was attached. Rubber hoses leading from the building supply water to the bulkhead and from the bulkhead to a drain provided the test fluid for the experiments. Attached to the bulkhead was the 1/16 inch stainless steel thin walled tube with inconel sheathed type K thermocouples (Omega KMQIN-020U-12) to read the inlet and outlet temperatures of the test fluid. The $1/16^{th}$ inch tube was used in order to minimize the heat transfer area, which increased the heat flux. Figure 5 shows a schematic of the bulkhead. The temperatures were read and collected using a dual input thermocouple reader (Omega H509R Dual Input D Thermometer), and the flowrate through the bulkhead was measured with a rotameter (Cole-Parmer A-32461-40) positioned on the exit side of the apparatus.

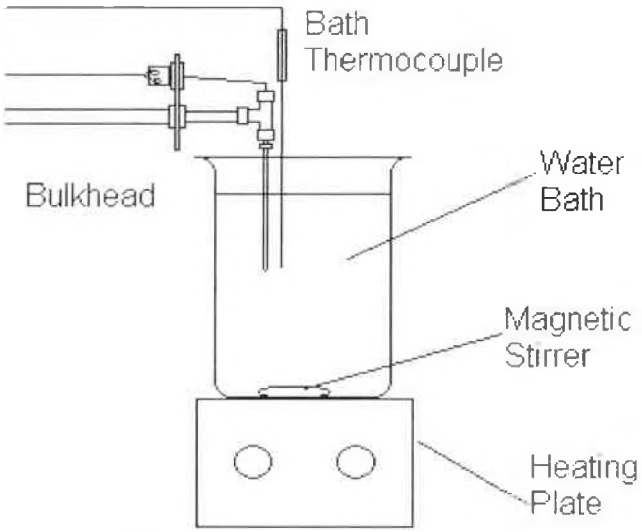

Figure 6: Stirred Water Bath Apparatus.

Stirred Water Bath

The first configuration of the liquid immersion heat exchanger tested the heat transfer capability of water. A stirred water bath, heated by a heated stir plate, provided energy to the immersed tube. The bath temperature was varied in this series of experiments, and the heat flux was calculated based on the temperature change of the test fluid. The main objective of using this set up was to ensure that the water was well stirred, which maximized the heat transfer coefficient. Its main drawback is that the maximum operating temperature is below 100°C, the boiling temperature of water. Figure 6 shows the stirred water bath apparatus.

Heat Conduction Tube

This configuration consisted of a 12 inch quartz tube (closed at one end) with the EDM inside. Heating was accomplished by a 12 inch tube heater

(Lindberg 55035A). The mixture was heated to melting and experiments were run at different temperatures (260°C to 537°C) and immersion lengths (2 to 10 inches). As stated before, EDM is limited to a maximum temperature of 565°C before decomposition to NO_x begins. It should be noted that the salt was not stirred so heat transfer occurred only via conduction and buoyant convection. In addition to EDM, water was also used in the conduction tube to compare the two heat transfer fluids. A simple schematic of the conduction tube apparatus is given in Figure 7.

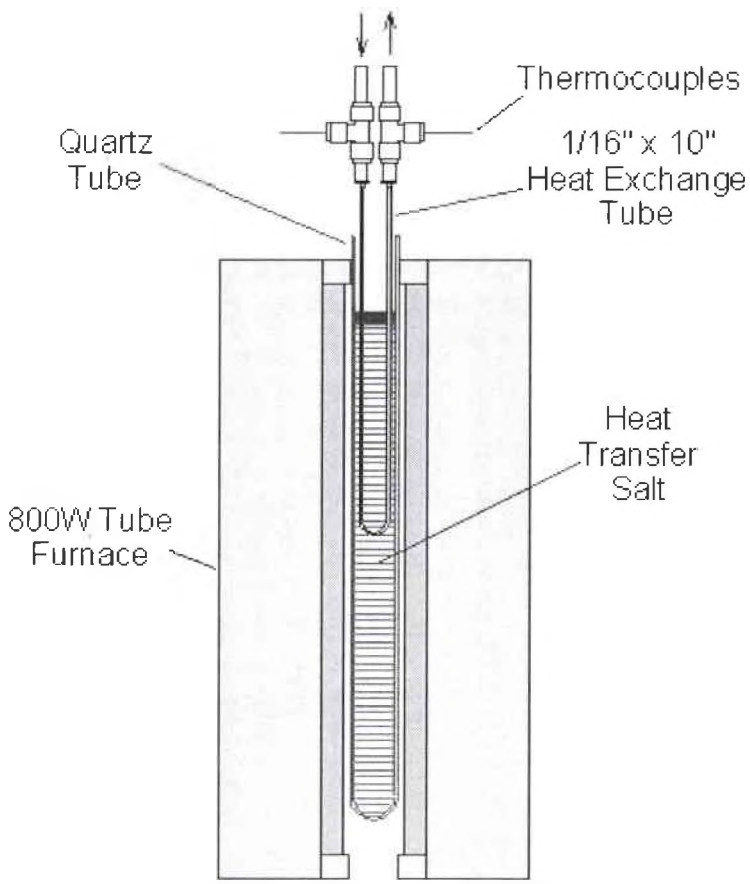

Figure 7: Schematic of Conduction Tube Apparatus.

Stirred Eutectic Drawsalt Bath

The current design of the liquid immersion heat exchanger has the following overall configuration. A 0.8 ft^3 kiln (Skuttle KS-614-3) heated water to near boiling and the EDM to its melting point, approximately 120°C [12]. The EDM was tested from 288°C to 482°C, and could not be taken higher due to physical restraints of the kiln heater. Additionally, the water was tested between 50°C and 95°C. The test fluid ran through the thin walled 1/16th inch stainless steel pipe, which in turn, was lowered into the immersion bath. Finally, for agitation, a stirrer (IKA Model RW 16 Basic) mixed the EDM and water to

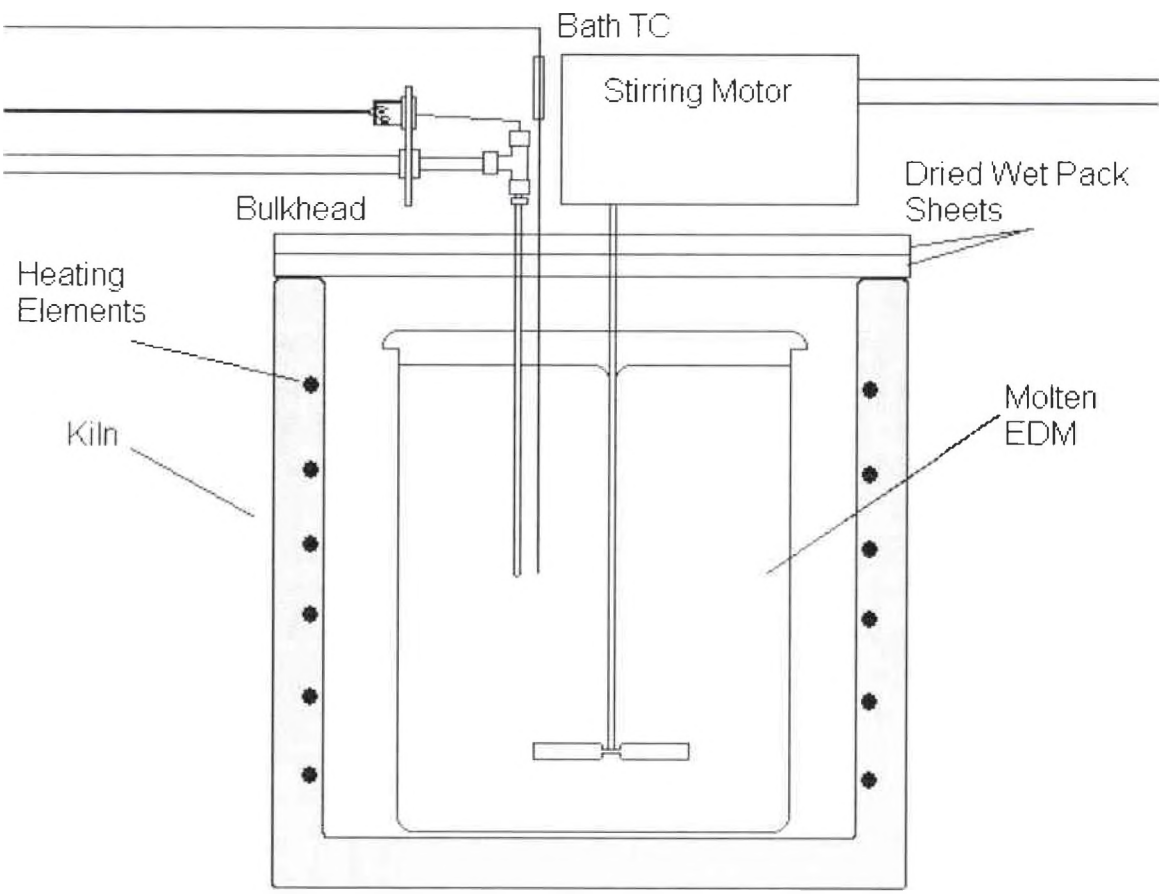

Figure 8: Schematic of Stirred Bath.

increase the heat transfer coefficient at the liquid solid interface. A general schematic of the agitated salt bath is given in Figure 8.

CHAPTER IV

HEAT TRANSFER MODEL

In the development of the mathematical model, it is important to understand the methods of heat transfer occurring around the defined system. With regard to the immersion bath experiment, there are several regions of different heat transfer characteristics. Going down the temperature gradient, the regions are: the bulk heat transfer fluid, the heat transfer fluid boundary layer, the solid EDM layer, the steel tube, the test fluid boundary layer, and the bulk test

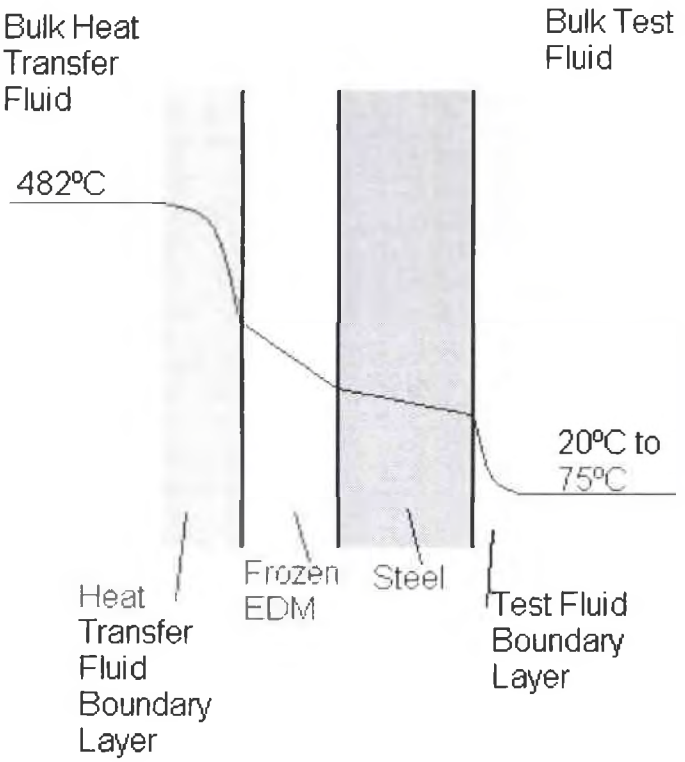

Figure 9: Schematic of Stainless Steel Tube, Frozen Salt Layer, and Thermal Boundary Layers.

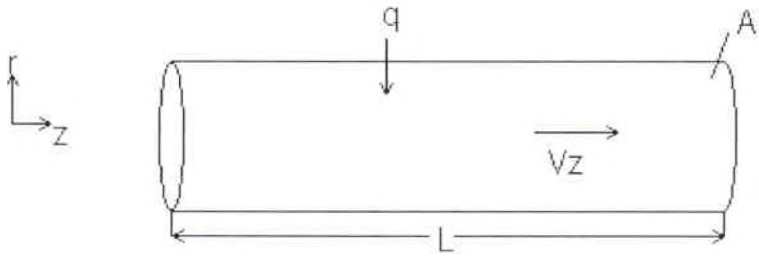

Figure 10: System of Concern for Modeling.

fluid as shown in Figure 9. It should be noted that the solid salt layer only occurs in the EDM immersion fluid.

The system of concern is the test fluid flowing at a velocity, v_z, through the heated section of a thin walled tube of some length, L, and a heat transfer surface area, A_0, along the outer surface of the flowing test fluid as shown in Figure 10.

Determination of heat flux within this system can follow a simple calculation using the first law of thermodynamics. A differential energy balance using the first law on an open system [13] results in the following equation:

$$d\overline{U} = \delta Q - \delta W + \sum_{in} H_{in}\delta n - \sum_{out} H_{out}\delta n \qquad (4.1)$$

where dU, the total internal energy, is equal to the heat input, δQ, minus the work output, δW, and any energy passing into or out of the system via mass transfer, $H_{in}\delta n$ and $H_{out}\delta n$. First, assuming constant density and steady state fluid and energy flow, the change in total internal energy of the system is zero. Since no mechanical work is being done on the system, this term also goes to zero. Thus Equation (4.1) reduces to

$$\delta Q = H_2 \delta n_2 - H_1 \delta n_1 \tag{4.2}$$

where δn_1 is the number of moles entering the system, δn_2 is the number of moles exiting the system in a differential period of time, δt, and H_1 and H_2 are the specific enthalpies of the incoming and outgoing fluid, respectively.

Enthalpy of a given material, H_i, can be found if the temperature, T_i, is known and the reference enthalpy, H_0, is known at a reference temperature, T_0. Mathematically, this is given by

$$H_i = H_0 + \int_{T_0}^{T_i} C_p dT \tag{4.3}$$

where C_p is the molar heat capacity of the material at constant pressure. Typically, the heat capacity can be taken as constant, but if not, it is represented as a function of temperature. Applying Equation (4.3) to the conditions at the entrance and exit of the system, the fluid enthalpies are given by:

$$H_1 = H_0 + C_p(T_1 - T_0) \tag{4.4}$$

$$H_2 = H_0 + C_p(T_2 - T_0) \tag{4.5}$$

where H_1 and T_1 are the enthalpy and temperature of the entrance stream, and H_2 and T_2 are the enthalpy and temperature of the exit stream, respectively. C_p is taken as constant since it does not change significantly over the temperature range (4186.8 J/kgK to 4193.0 J/kgK over the temperature range 20°C to 70°C) [14]. Applying Equation (4.4) and Equation (4.5) and accounting for the steady state condition, $\delta n_1 = \delta n_2 = \delta n$, Equation (4.2) becomes:

$$\delta Q = \delta n\{(H_0 + C_p(T_2 - T_0)) - (H_0 + C_p(T_1 - T_0))\}$$

$$\delta Q = \delta n C_p (T_2 - T_1) \tag{4.6}$$

Now dividing both sides of the equation by the time differential, δt, yields Equation (4.7).

$$\frac{\delta Q}{\delta t} = \frac{\delta n}{\delta t} C_p (T_2 - T_1) \tag{4.7}$$

or

$$\dot{Q} = \dot{n} C_p (T_2 - T_1) \tag{4.7a}$$

where $\dot{Q}$ is the heat flow rate and $\dot{n}$ is the molar flow rate. Finally, changing the heat capacity and molar flow rate from a per mole basis to a per mass basis and dividing Equation (4.7) by the heat transfer area yields the final governing equation for the flow system.

$$\dot{q} = \frac{\dot{m} \hat{C}_p (T_2 - T_1)}{A_0} \tag{4.8}$$

where $\dot{q}$ is the heat flux, $\dot{m}$ is the mass flow rate, $\hat{C}_p$ is the specific heat capacity, and A_0 is the heat transfer area at the outer surface of the surface. Note that Equation (4.8) determines heat flux assuming that no phase change takes place.

In both the heat conduction tube and the stirred baths, the bulk fluid remains isothermal under steady state conditions. This means that any energy that is removed by test fluid is replaced by the electrical heaters. However, since the amount of immersion fluid is large compared to that of the test fluid, the salt can act as a thermal energy reservoir for heat transfer.

The immersion fluid boundary layer has two possible methods of heat transfer. For the conduction tube, heat conduction and free convection occurs.

In this mechanism heat flows from the bulk fluid into the boundary layer, which then interacts with the solid surface. This solid-fluid interaction for heat transfer can be described by Newton's law of cooling, given in Equation (4.9).

$$\dot{q} = h(T_{\infty} - T_0) \tag{4.9}$$

where h is the heat transfer coefficient, and T_8 - T_0 is the temperature driving force. Free convection occurs because of density differences between hot and cold regions in the molten EDM or water. As a result of density differences the fluid moves, however rapid mixing does not occur. These two methods occur in the bulk immersion fluid and are less efficient at transmitting heat than forced convection.

The steel layer is from $r_0 < r < r_1$, while the solid salt layer is from $r_1 < r < r_2$, in both of which the mechanism is conduction. The outer salt layer is of variable thickness according to bath temperature and always has the outer temperature at the melting temperature of the EDM (120°C) [12]. The frozen salt region only occurs while using the EDM immersion fluid. Its formation is due to the temperature of the skin of the steel being lower than that of the fusion temperature of the EDM, and its thickness also depends on the steel skin temperature. The frozen salt creates an insulating layer, which interferes with the heat transfer, around the steel. Heat flux through this layer is dependent on the thermal properties of the frozen salt and its thickness.

The steel tube provides resistance to heat flow as well. The mechanism of heat transfer in the steel tube is conduction, which is based on thermal properties and thickness, like the frozen salt layer. However, its thickness is not

a strong function of temperature (minimal expansion may occur at high temperatures), so it is assumed constant. As a result, the heat flow through this layer is easily modeled, using Fourier's Law of heat conduction as shown in Equation (4.10) [15].

$$q_r = -k\frac{dT}{dr} \tag{4.10}$$

where k is the thermal conductivity and dT/dr is the temperature gradient. For the steel layer and the solid EDM layer, conduction is only considered in the radial direction.

After conduction through the steel, heat enters the test fluid boundary layer which carries heat via conduction and convection into the test fluid. Typical Reynolds numbers for this experiment ranged from 100 to 1000 within the stirred bath and 24,000 to 30,000 for the test fluid. This method of heat transfer is well documented as a Nusselt correlation for pipe flow. The Nusselt number is defined as in Equation (4.11) [15].

$$Nu = \frac{hD}{k} = \frac{\text{convective heat transfer}}{\text{conductive heat transfer}} \tag{4.11}$$

A more general description of what the Nusselt number represents is the ratio of the convective heat transfer to the conductive heat transfer of a given substance. Thus, for Nu > 1, convection dominates heat transfer, and for Nu < 1 conduction dominates [15]. For highly turbulent pipe flow (Re > 20,000) a representative Nusselt number correlation for tube flow is as shown in Equation (4.12) [14].

$$Nu = K(\mathrm{Re})^{0.8}(\mathrm{Pr})^{1/3}(\phi)^{0.14} = 0.023\left(\frac{DG}{\mu_b}\right)^{0.8}\left(\frac{\hat{C}_p\mu}{k}\right)^{1/3}\left(\frac{\mu_b}{\mu_0}\right)^{0.14} \tag{4.12}$$

where μ_b, the viscosity of the bulk fluid, $\hat{C}_p$, the specific heat capacity of the fluid, μ_0, the viscosity of the fluid at the arithmetic mean temperature of the bulk fluid and steel skin temperatures, and *k* is the thermal conductivity of the fluid at the arithmetic mean temperature. The ratio of μ_b/μ_0 accounts for viscosity variations within the film layer. The Nusselt correlation also accounts for the rate of fluid flow through the Reynolds number, DG/μ_b, where *G* is the mass velocity [14]. This allows for the estimation of the heat transfer coefficient on the test fluid side.

For the heat transfer coefficient of the boundary layer on the heat transfer fluid side, a different correlation must be used. In this case, fluid flowing past a tube is being analyzed. Past research by Churchill and Bernstein has shown that for this configuration another Nusselt correlation can be used [16].

$$Nu = 0.30 + \frac{0.62\,\mathrm{Re}^{1/2}\,\mathrm{Pr}^{1/3}}{\left[1+(0.40/\mathrm{Pr})\right]^{1/4}}\left[1+\left(\frac{\mathrm{Re}}{282000}\right)^{5/8}\right]^{4/5} \qquad (4.13)$$

Equation (4.13) is valid for Re*Pr > 0.40 and can predict heat transfer coefficients for flow past a submerged tube as shown in Figure 11 [16]. The configuration of the experimental system does not match this model precisely; however other considered models gave similar results. Equation (4.13) considers only linear flow, whereas the liquid immersion heat exchanger will be stirred angularly. The tangential velocity of the fluid flowing around the outside of the test piece is used in the Reynolds number calculation. The Reynolds number calculation is different from the standard calculations and is represented in Equation (4.13a).

$$\mathrm{Re} = \frac{v_\theta D_1 \rho}{\mu} \qquad (4.13a)$$

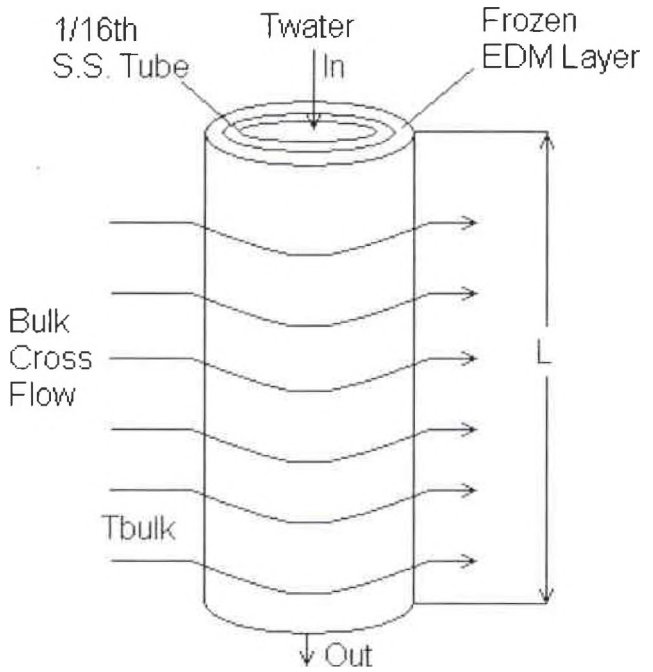

Figure 11: Cross Flow Estimation of System.

where v_θ is the tangential velocity, D_1 is the outside diameter of the test piece, ρ is the fluid density, and μ is the viscosity.

The actual modeling of heat flux through these regions is complex since it combines both conduction and convection. With respect to the system, the temperature will change along the immersed length. Thus, heat flux decreases as the axial position increases. Also, since the test fluid is at a lower temperature than the heat source, natural thermal gradients are established in the radial direction. These two phenomena acting together describe the overall temperature profile as being a function of both z and r (T = f(r,z)). This can be further supported by looking at the equation of energy as derived in Bird, Stewart, and Lightfoot [15].

$$\rho \hat{C}_p \left(\frac{\partial T}{\partial t} + v_r \frac{\partial T}{\partial r} + \frac{v_\theta}{r} \frac{\partial T}{\partial \theta} + v_z \frac{\partial T}{\partial z} \right) = k \left[\frac{1}{r} \frac{\partial}{\partial r} \left(r \frac{\partial T}{\partial r} \right) + \frac{1}{r^2} \frac{\partial^2 T}{\partial \theta^2} + \frac{\partial^2 T}{\partial z^2} \right] \quad (4.14)$$

where ρ is the density, $\hat{C}_p$ is the heat capacity, T is temperature, t is time, r, θ, and z are the radial coordinates with which T varies, k is the thermal conductivity, and v is the velocity in the r, θ and z directions. When simplified for this system, the following partial differential equation is developed.

$$\alpha \frac{\partial T}{\partial z} = \frac{1}{r} \frac{\partial T}{\partial r} + \frac{\partial^2 T}{\partial r^2} \quad (4.15)$$

where α is the collection of constant physical properties and the bulk velocity in the z-direction as shown in Equation (4.15a).

$$\alpha = \frac{\rho \hat{C}_p v_z}{k} \quad (4.15a)$$

Equation (4.15) describes heat conduction through the salt and steel layers. The particular solution derivation is beyond the scope of this thesis. However, using Maple Release 5.1 [18] the general solution can be found as seen in Equation (4.16).

$$T(r,z) = C3 \exp\left(\frac{\beta z}{\alpha} \right) * \left[C1 BesselJ\left(0, \sqrt{-\beta} r\right) + C2 BesselY\left(0, \sqrt{-\beta} r\right) \right] \quad (4.16)$$

where C3, C1, and C2 are constants of integration based on the boundary conditions, and β is a boundary condition for the z-direction. BesselJ and BesselY are Bessel functions of the first and second kind, respectively, which satisfy the Equation (4.16a).

$$x^2 y'' + xy' + (x^2 - v^2) y = 0 \quad (4.16a)$$

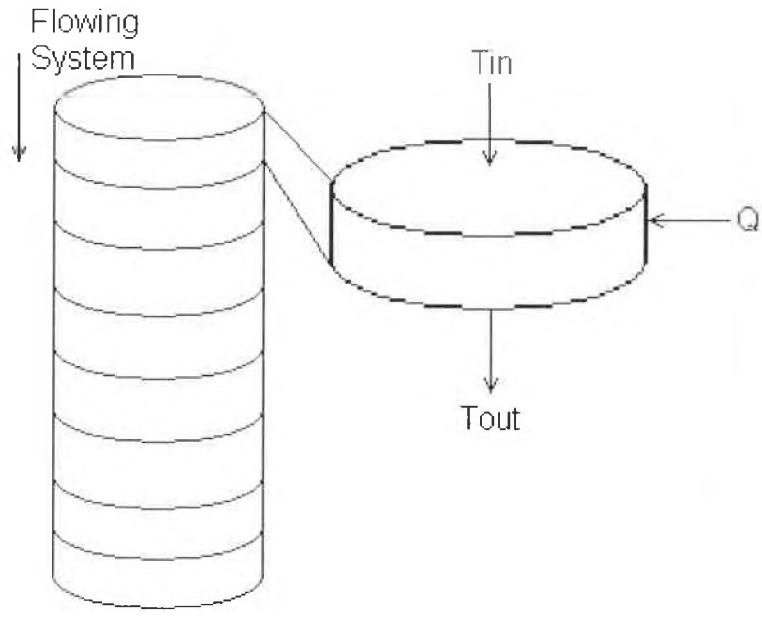

Figure 12: Discretization of Flowing System.

The argument of the Bessel function as given in Equation (4.16) denotes first the order of the function followed by the point to be evaluated. In particular, the zero indicates that the Bessel functions are zero order, and the second term indicates the radial position at which the functions are evaluated. Bessel functions are complicated infinite series summations and are involved in the solution to Equation (4.15). This solution is much too complex for the model and makes it difficult to introduce convective terms to account for the boundary layers and to apply the boundary conditions.

For a simpler model, discretization is used to divide the test fluid within the tube into cross sections of finite height, Δz. This is shown in Figure 12. Over this small change in z, it is assumed that the temperature is only a function of radial position such that energy equation becomes Equation (4.17) [15].

$$\frac{d}{dr}(rq_r) = 0 \tag{4.17}$$

where q_r is the heat flux in the r-direction. Integration of this equation shows that the product rq_r is constant. The constant of integration is the product of the inner radius and the heat flux at the inner radius, r_0q_0. This allows the application of Fourier's Law of heat conduction, which states that the heat flux is proportional to the temperature gradient as shown in Equation (4.18) [15].

$$q_r = -k\frac{dT}{dr} \tag{4.18}$$

Each section of the system must be solved separately. For the steel layer, $r_0 < r < r_1$, and the frozen EDM layer, $r_1 < r < r_2$, Equation (4.18) applies:

$$-k_{steel}\, r\frac{dT}{dr} = r_0 q_0 \tag{4.18a}$$

$$-k_{frozen\ salt}\, r\frac{dT}{dr} = r_0 q_0 \tag{4.18b}$$

For the water bath, the boundary conditions will be on the skin surfaces of the steel tube. This means that $T = T_0$ at $r = r_0$ and $T = T_1$ at $r = r_1$. Applying these two boundary conditions to the system yields Equation (4.19) below.

$$T_1 - T_0 = r_0 q_0 \left(\frac{\ln(r_1\ r_0)}{k_{steel}} \right) \tag{4.19}$$

For the salt bath, an extra boundary condition is necessary to account for the salt layer forming on the steel pipe. In this case, $T = T_0$ at $r = r_0$, $T = T_1$ at $r = r_1$, and $T = T_2$ at $r = r_2$. Applying these boundary conditions results in Equation (4.20) below.

$$T_2 - T_1 = r_0 q_0 \left(\frac{\ln(r_2 / r_1)}{k_{frozen\ salt}} \right) \tag{4.20}$$

These two equations govern the heat conduction within the steel pipe and the frozen salt layer. However, for boundary layers on the inside of the steel tube and the outside of the salt layer, heat transfer coefficients must be taken into account. Applying Newton's law of cooling to these two boundary layers results in the following equations.

$$T_0 - T_{in} = \frac{q_0}{h_0} \tag{4.21}$$

$$T_\infty - T_2 = \frac{q_2}{h_2} = \frac{q_0}{h_2} \frac{r_0}{r_2} \tag{4.22}$$

where T_{in} is the temperature of the inlet stream and T_8 is the temperature of the bulk heat transfer fluid. Using Equations (4.19) through (4.22) and then solving for the heat flow yields Equation (4.23), which is used for the salt experiments.

$$Q_0 = \frac{2\pi L (T_\infty - T_{in})}{\frac{1}{r_0 h_0} + \frac{\ln(r_1 / r_0)}{k_{steel}} + \frac{\ln(r_2 / r_1)}{k_{frozen\ salt}} + \frac{1}{r_2 h_2}} \tag{4.23}$$

where Q_0 is the heat flow into the system, and L is the tube length. Similarly, for the water experiments, which have no salt layer, Equation (4.24) is used.

$$Q_0 = \frac{2\pi L (T_\infty - T_{in})}{\frac{1}{r_0 h_0} + \frac{\ln(r_1 / r_0)}{k_{steel}} + \frac{1}{r_1 h_1}} \tag{4.24}$$

Using Equation (4.23) or Equation (4.24), the total heat flowing into the water can be evaluated.

The actual model uses discretized cross sections to determine the heat flux and temperature change of the test fluid. Equation (4.23) or (4.24) is used to determine first how much heat is transferred to the test fluid based on the inner diameter of the pipe after replacing L with Δz. Following this calculation, the temperature change of the fluid is determined by Equation (4.7a). These sequential calculations are performed along the entire heated length to find the total heat flux and the final temperature of the last fluid disc. To sequentially determine the temperature at the exit of the disc, Equation (4.25) is used.

$$T_i = \frac{(Q_i)}{\dot{m}\hat{C}_p} + T_{i-1} \tag{4.25}$$

where T_i and T_{i-1} are the outlet and inlet stream temperatures and Q_i is the heat flow into the fluid element. The summation of these individual heat flows divided by the heat transfer area, or using Equation (4.8) determines the overall heat flux for the system. This was done in both Microsoft Excel and Microsoft Visual Basic 6.0 [19]. The code for the Visual Basic program is given in Appendix A.

CHAPTER V

RESULTS AND DISCUSSION

Gas-Solid Heat Transfer

Initially, gas-solid heat transfer experiments were conducted to observe the ability of a gaseous heat transfer fluid. Figure 13 gives the temperature dependence of heat flux to a 1/16th inch stainless steel tube in stagnant air, and Figure 14 shows the same for a 1/4 inch copper tube in air, and in both the primary mode of heat transfer is conduction.

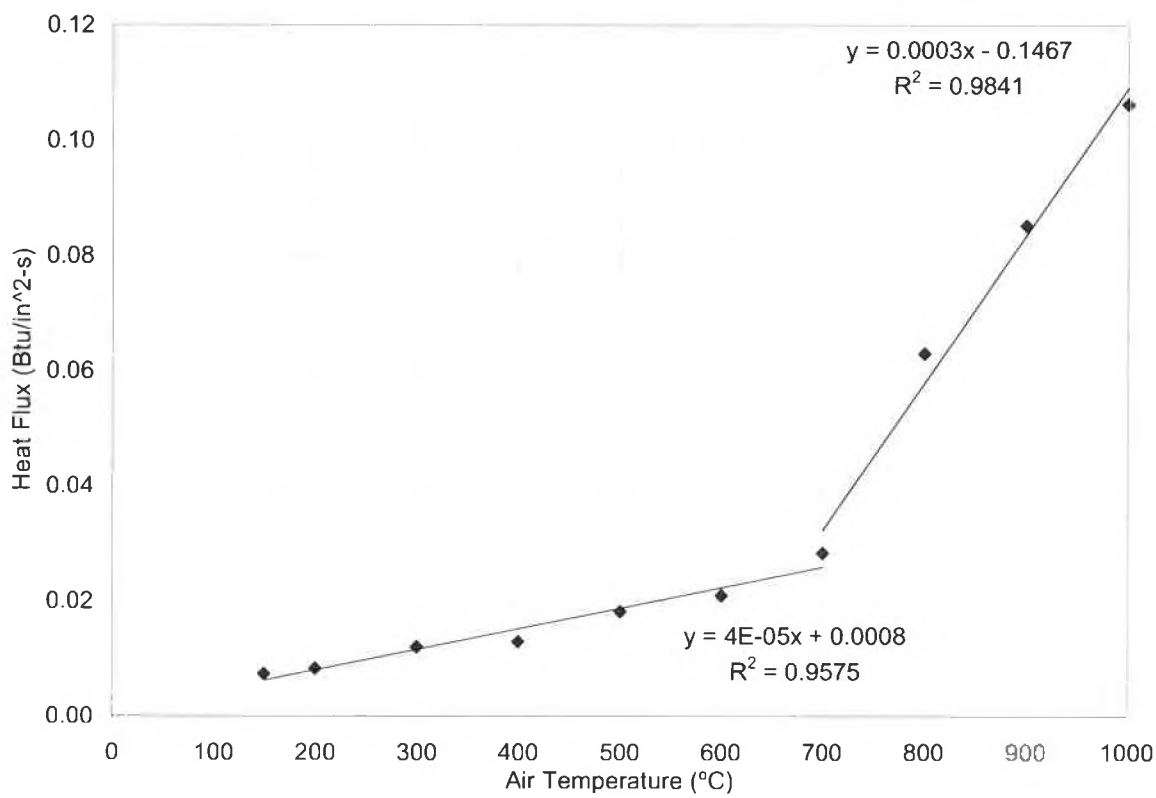

Figure 13: Heat Flux of 1/16 inch Stainless Steel Tube.

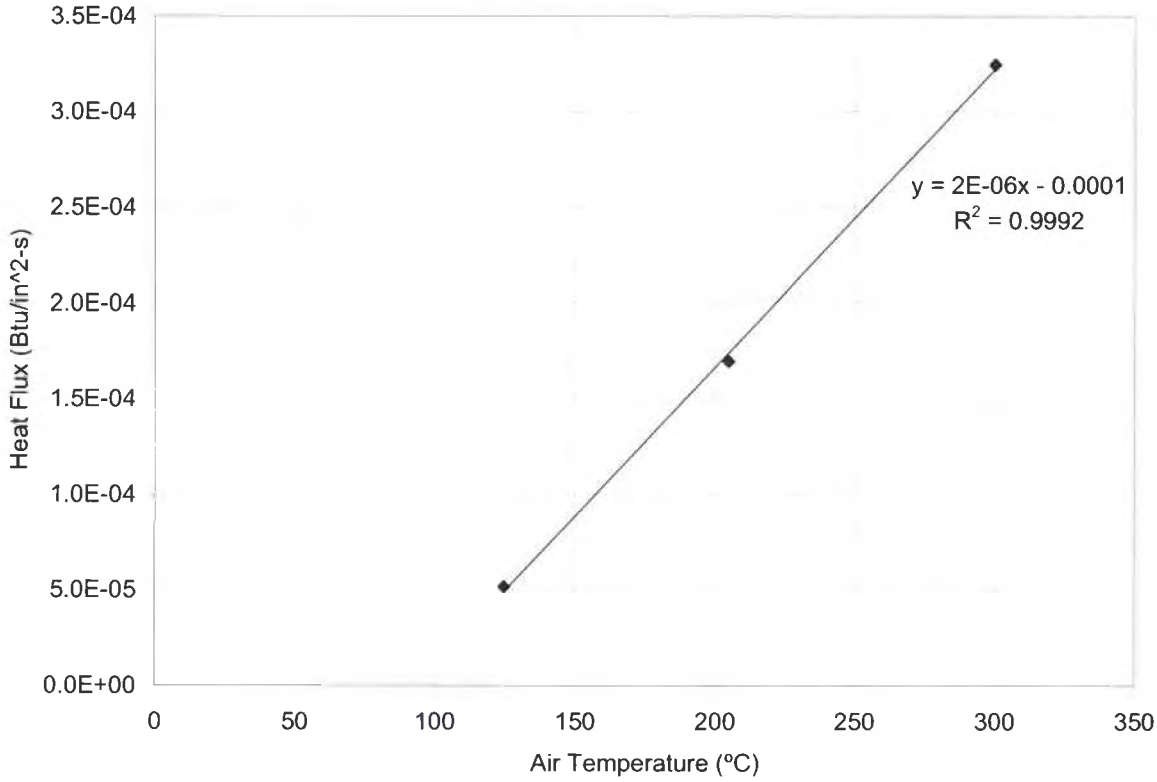

Figure 14: Heat Flux of a 1/4 inch Copper Tube.

As can be seen in Figure 13 the maximum heat flux achieved by the gas-solid interface is 0.106 Btu/in^{2}s. A noticeable increase in the heat flux rate occurs at about 700°C, which is attributed to a change of the dominant heat transfer mechanism from conduction to radiation. Also, from Figure 14 the highest achieved heat flux was 3.24*10^{-4} Btu/in^{2}s for the copper tube. The copper tube did not perform as well since the heat transfer area was larger because of the larger tube diameter. This larger diameter increases the heat transfer area, which decreases the total heat flux. However, both of these experiments have very low heat fluxes due to a gas-solid interface and promote the search for a better heat transfer fluid.

Stirred Water Bath

Figure 15 shows the correlation of heat flux with bath temperature within the stirred water bath in a beaker. As expected from Equation (4.8), there is a linear relationship between heat flux and bath temperature. These results were encouraging, indicating that the potential heat flux that the salt bath could produce would be significant. Since the water bath results have a maximum of 0.460 Btu/in^{2}s at only 95°C, the salt bath should have a much higher flux. Using the linear regression from the stirred water bath, the salt bath, which has a maximum operating temperature of 510°C, could produce a heat flux on the order of 2.64 Btu/in^{2}s.

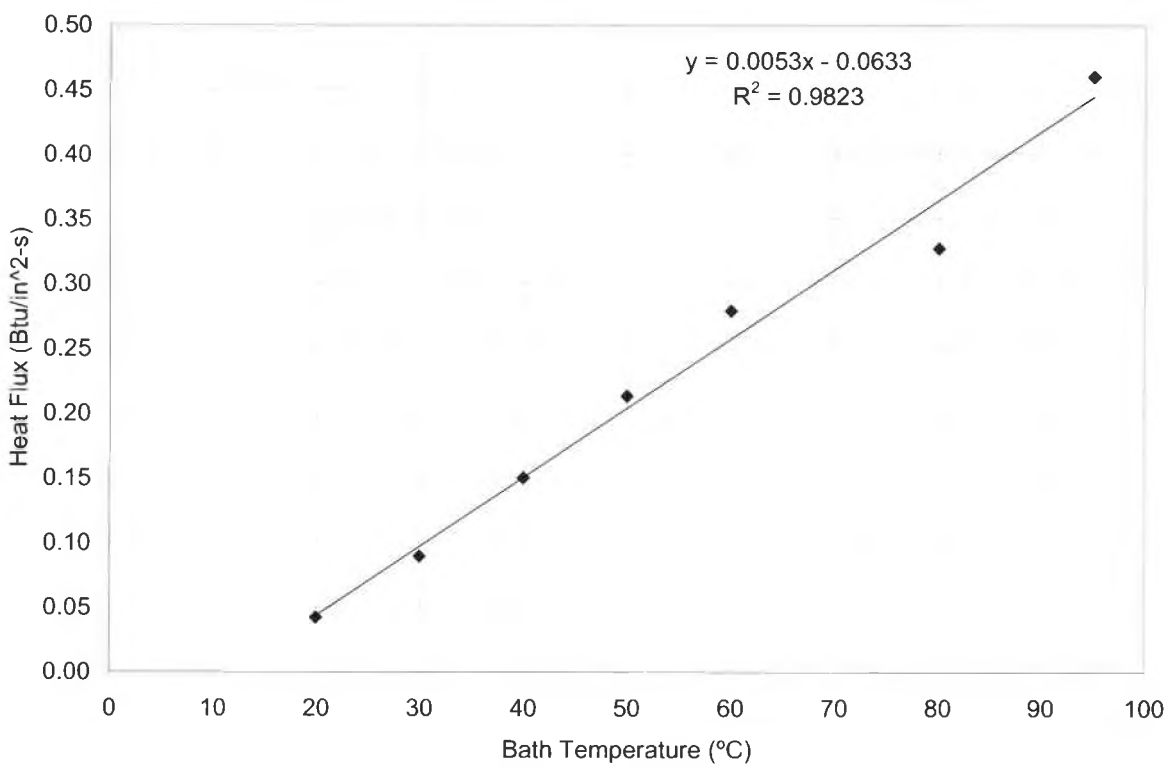

Figure 15: Heat Flux of Stirred Water Bath in Beaker.

Conduction Tube Experiments

Figure 16 shows the heat flux produced from the EDM in the heat conduction tube configuration.

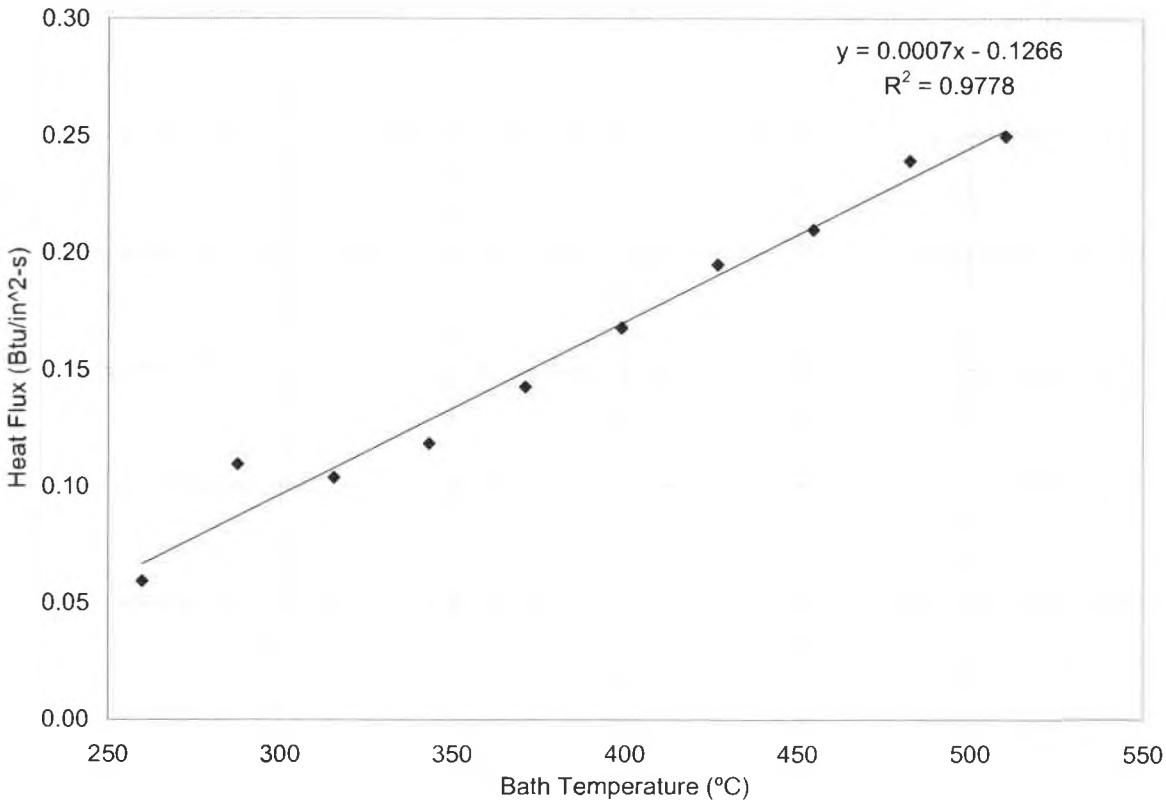

Figure 16: Heat Flux of EDM in Conduction Tube at 10 inches of Immersed Length and 0.460 L/min (19.9 ft/s).

In the conduction tube configuration, the EDM did not perform as expected, reaching a maximum heat flux of about 0.250 Btu/in^{2}s at 510°C where it was predicted to reach a maximum of 2.64 Btu/in^{2}s. There are some explanations for this discrepancy. First, the bulk motion of the fluid in the conduction tube is very limited, and any movement occurs by free convection. Thus, the mode of heat transfer is dominated by conduction, which is not as an efficient mode of transport when compared to convection. Second, a large amount, upwards of a

few millimeters, of solid salt formed along the length of the immersed tube, which further added to the limitations of heat conduction. Third, the initial comparisons between the two heat transfer fluids were carried out by comparing stirred water to stagnant EDM. This comparison is invalid since these are two different modes of heat transfer.

A second set of conduction tube experiments was performed using water as the heat transfer fluid. As with the EDM, only conduction and free convection occurred during these experiments. Figure 17 shows the resulting heat flux from the water in conduction tube experiments. As expected, the performance of the water in the conduction tube heat exchanger was very poor when compared to that of the stirred water bath. The maximum achieved heat flux was 0.100

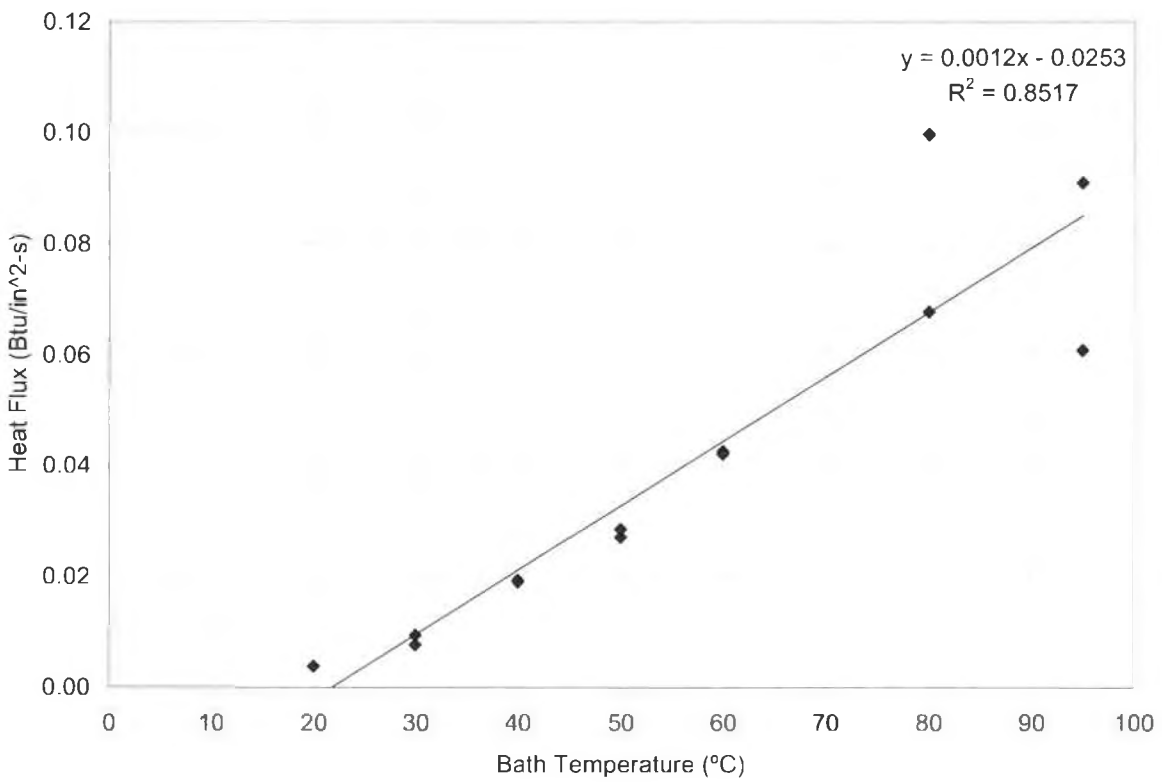

Figure 17: Water in Conduction Tube at 10 inches of Immersed Length and 0.460 L/min (19.9 ft/s).

Btu/in^{2}s at 80°C. A comparison of the two water experiments and the EDM experiment was performed to obtain an estimation of what a stirred salt bath could achieve. By taking the magnitude of the ratio of the stirred water bath data and the conduction tube water bath data and multiplying that factor by the conduction tube EDM data resulted in the estimation of the maximum heat flux for a stirred salt bath configuration. Figure 18 below shows what the stirred salt bath could potentially reach. A summary of the preliminary data is given in Table 1, which shows the maximum possible heat flux that could be achieved by a stirred salt bath.

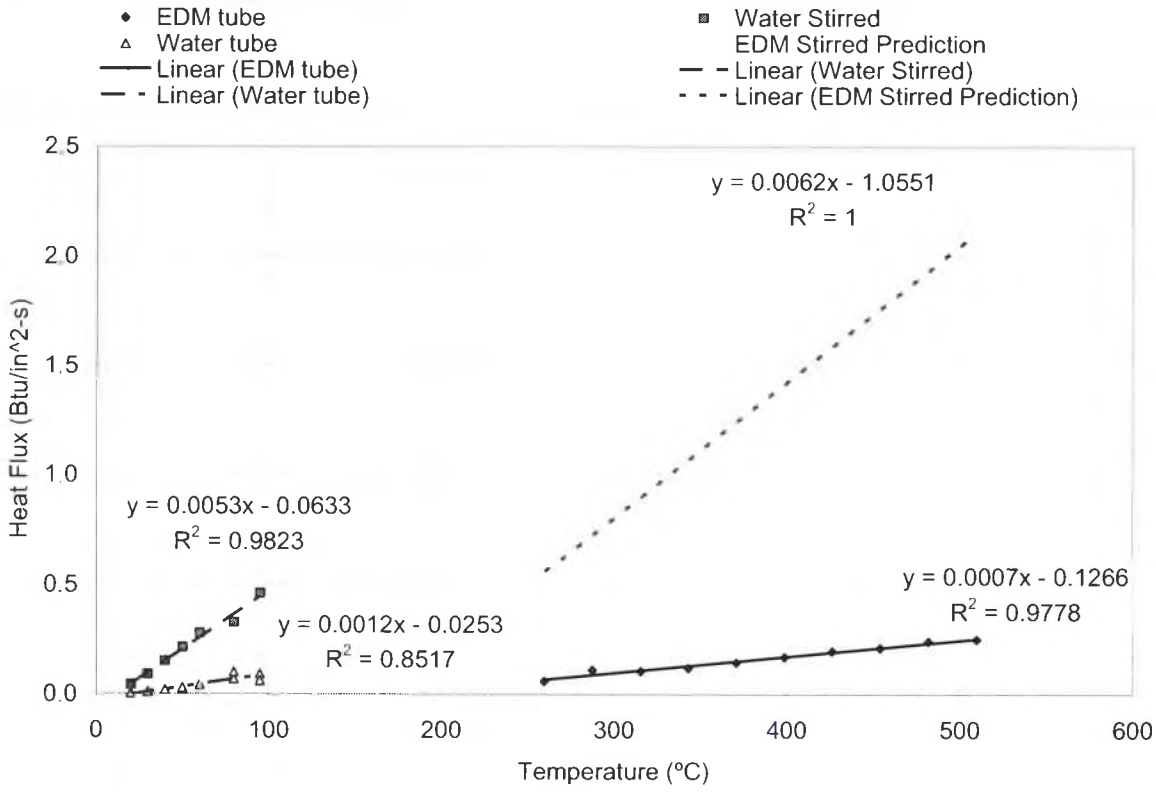

Figure 18: Prediction of Heat Flux of Stirred EDM Bath Based on Water Data.

Table 1: Preliminary Heat Transfer Results:

Heat Transfer Fluid	Maximum Heat Flux (Btu/in2s)	Temperature of Max Heat Flux (°C)
Air	0.106	1000
Water (stirred)	0.460	95
Water (tube)	0.100	80
EDM (tube)	0.556	482
EDM (stirred estimated)	2.08	510

Stirred Bath Experiments

At this point it was determined that a stirred salt bath should be constructed for the purposes of testing the performance of EDM as a heat transfer medium under convective conditions. Thus, the kiln configuration was constructed and tested with both water and EDM. The water experiments in the kiln showed similar results, given in Figure 19, as the previous stirred water bath

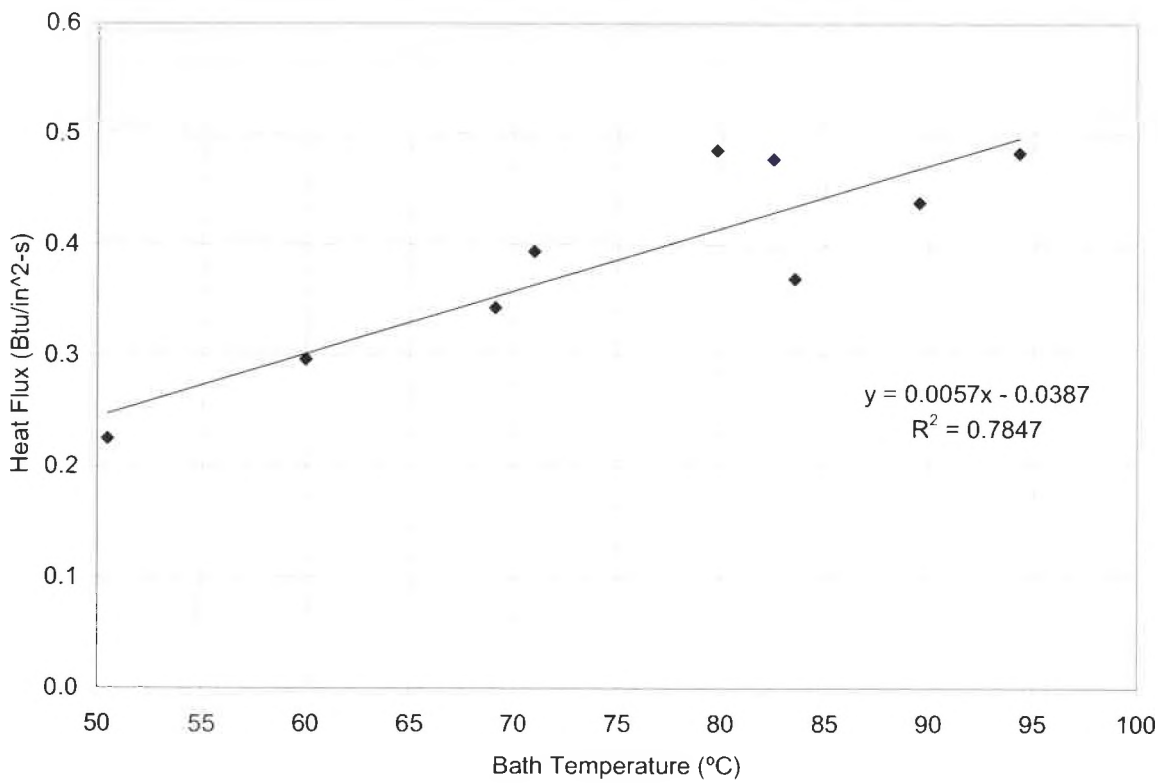

Figure 19: Heat Flux of Stirred Water Bath at Six inches of Immersed Length.

had shown. On the average, the volumetric flowrate of water was 0.407 ±0.016 L/min (17.6 ft/s). The EDM experiments gave positive results for the data collected from 288°C to 482°C and those results are shown in Figure 20. Here the maximum heat flux obtained was 1.65 Btu/in^{2}s at 468°C with a water flowrate of 0.435 L/min (18.8 ft/s). The relationship between heat flux and bath temperature should not be linear according the model described in Chapter IV. Equation (4.23) shows a direct linear relationship between the bath temperature, T_8, and heat flow. However, the heat transfer coefficients, h_1 and h_2 are temperature dependent and will change with

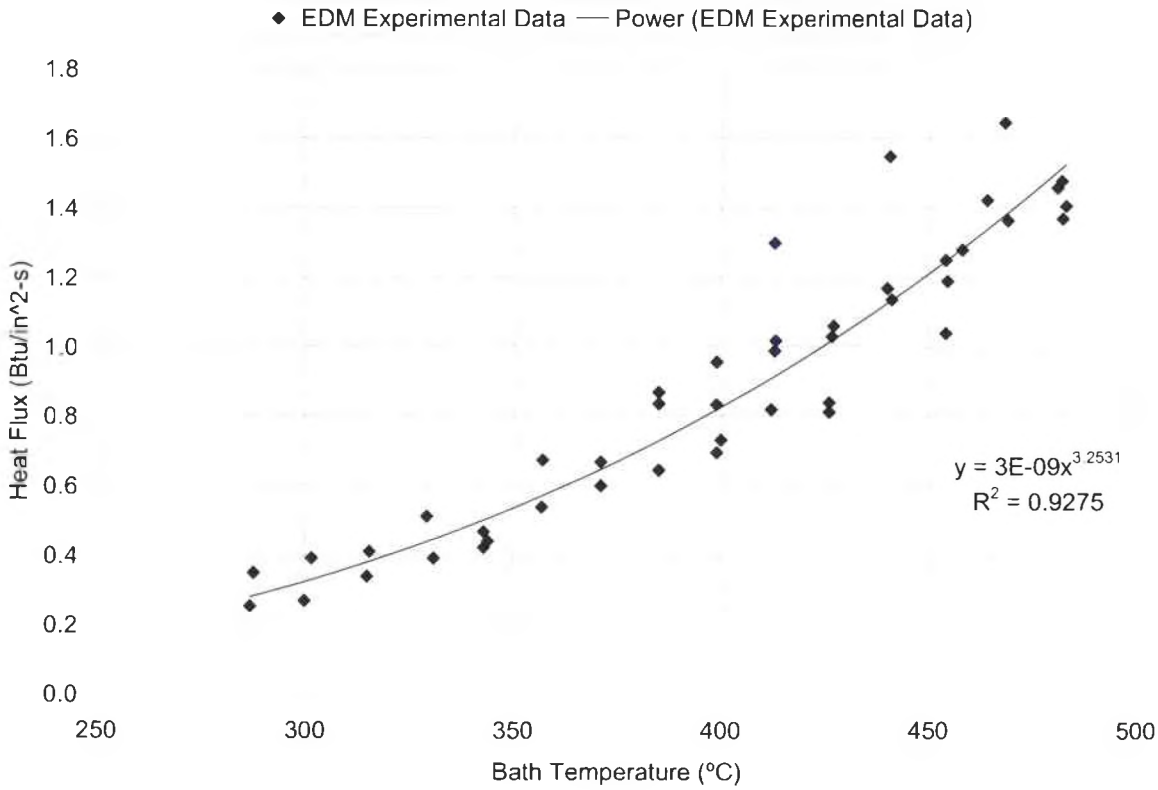

Figure 20: Heat Flux Results from EDM in Kiln Salt Bath at 6 inches of Immersed Length and Varied Flowrates.

Table 2: Stirred Bath Heat Transfer Results:

Heat Transfer Fluid	Maximum Heat Flux (Btu/in2s)	Temperature of Max Heat Flux (°C)
water	0.483	94.3
EDM	1.65	468

bath temperature. This would create a slight curvature to the data. Table 2 summarizes the results from the two heat transfer fluids.

Model Validation

For future application a model, as described by Equation (4.23) or Equation (4.24) and Equation (4.25), was created to predict possible heat flux of

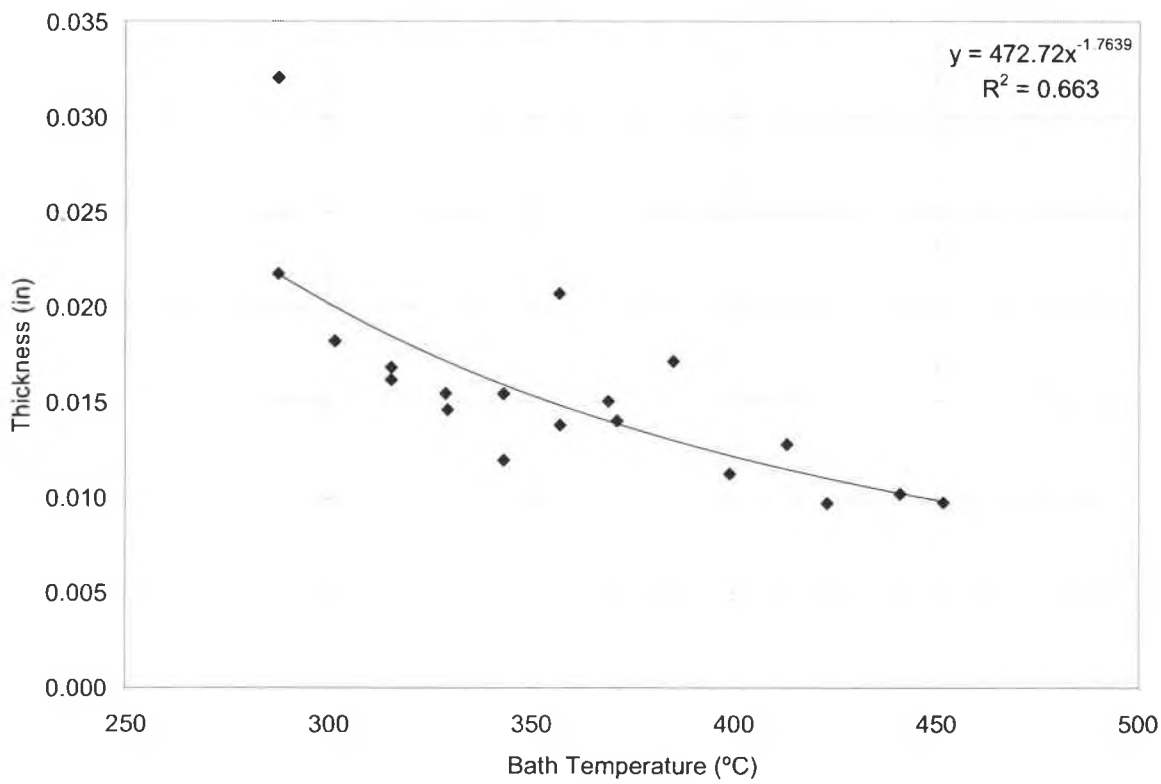

Figure 21: Frozen EDM Thickness at Varied Salt Bath Temperatures with Power Law Curve Fit.

the immersion salt bath. There were some complications in the real system, which were later applied to the final model. One was the thickness of solid EDM layer that forms on the test piece. These thicknesses were measured at different bath temperatures and the data were fitted with a power law curve. This would allow for the prediction of the frozen EDM thickness as a function of bath temperature to account for heat transfer resistances. The measured thickness as a function of temperature is shown in Figure 21.

Using the model for the same set of conditions (bath temperature, volumetric flowrate, etc.) the data from both the EDM and water baths were plotted with the predicted data of the model. Figure 22 shows the stirred water

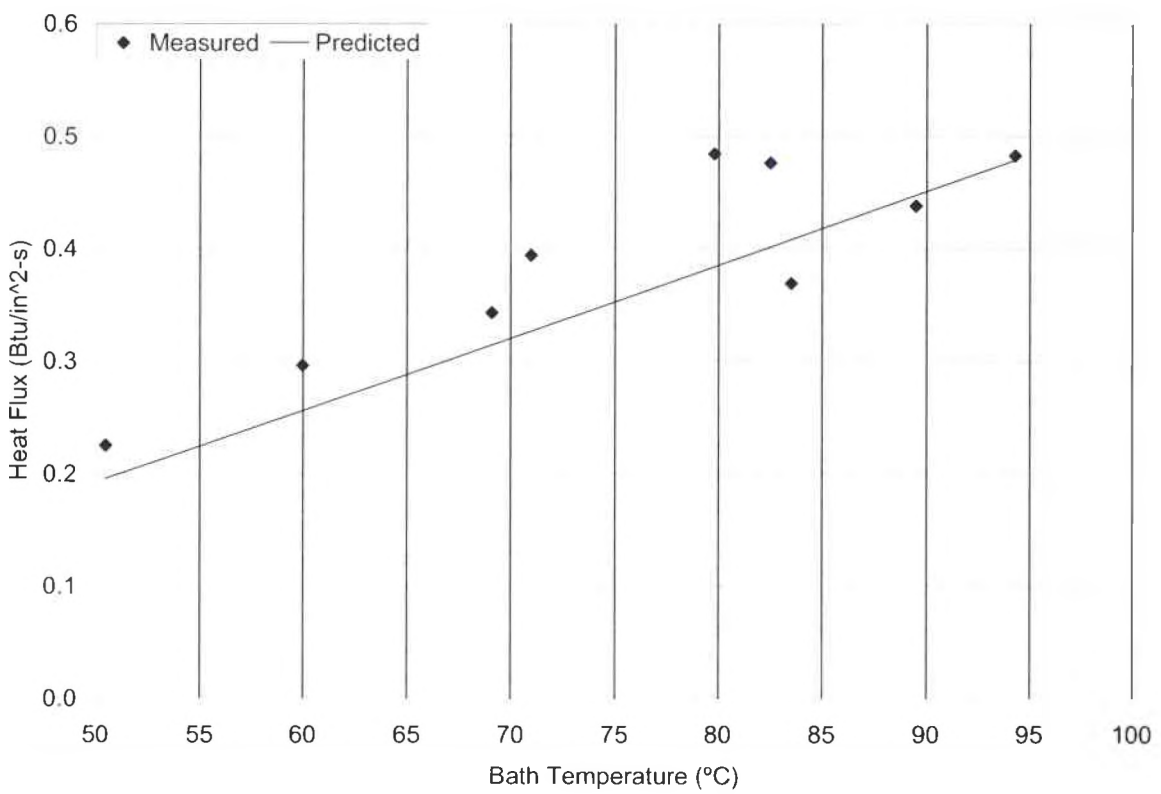

Figure 22: Heat Flux of Stirred Water Experiment with Model Predicted Behavior.

bath experimental results compared with the model. The predicted values have a good agreement with the experimental data. An analysis of the residuals gives a 90% confidence interval of -0.0330 $\pm$0.0240 Btu/in^{2}s. This means that on average the model will under predict the data. The scatter of the data from the model suggests a discrepancy which is attributed to the fluctuations in the volumetric flowrate. Figure 23 displays the heat flux results of the stirred EDM bath and the predicted values. Here the model agrees well with higher temperatures, but not with the low temperatures. Analysis of these residuals gives a 90% confidence interval of 0.172 $\pm$0.0432 Btu/in^{2}s, which shows that on average the model over predicts the data.

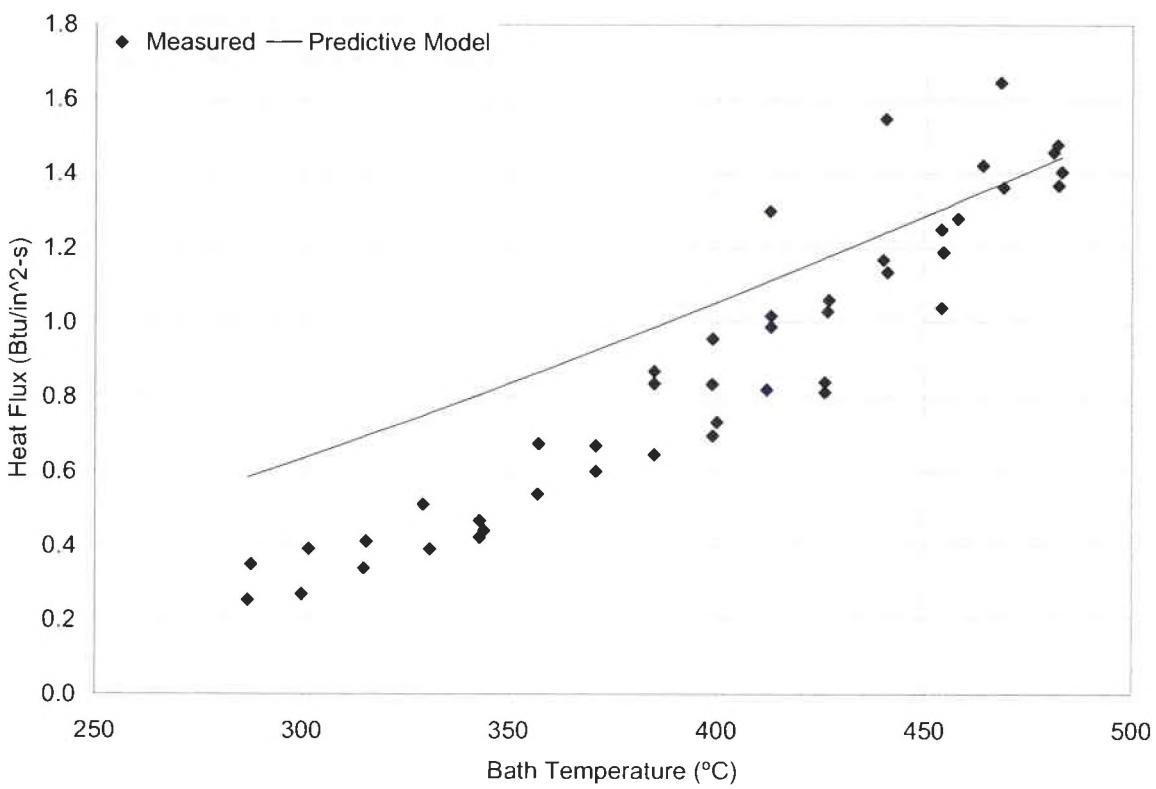

Figure 23: Heat Flux of Stirred EDM Experiment with Model Predicted Behavior at Six Inches of Immersed Length.

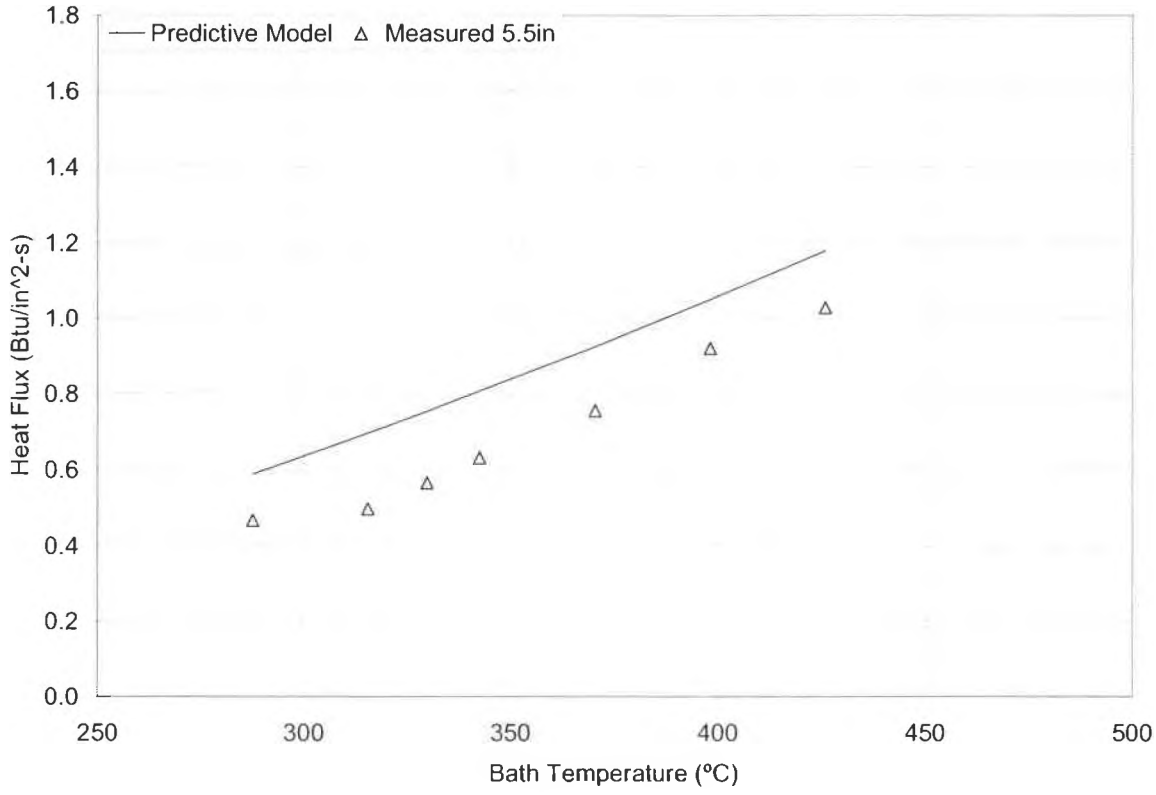

Figure 24: Heat Flux of Stirred EDM Experiment with Model Predicted Behavior at 5.5 Inches of Immersed Length.

The water bath shows good correlation with the model, however, the lower temperatures of the stirred EDM bath do not agree as well. There may be a few reasons behind this discrepancy. The first of these reasons may be due to the placement of the thermocouples. If the thermocouples were placed above the immersion level then an inaccurate reading of the temperature change would result. The immersion bath was operated again with the linear distance between the thermocouples changed to 5.50 inches. This resulted in higher heat flux at lower temperatures as shown in Figure 24. The model and the experimental values show good correlation, and analysis of the residuals gives a 90% confidence interval of 0.162 $\pm$0.0184 Btu/in^{2}s. This implies that the model over

predicts the data for the stirred EDM bath. A second reason could be the limited knowledge of the thermal properties of the EDM. Some of the properties such as viscosity and density were given as functions of temperature [12]. However, the heat capacity and thermal conductivity were given as constants at 427°C. It could be supposed that the heat capacity does not change significantly over the operating temperatures of the EDM, much like water does not. However, the thermal conductivity of most liquids increases with increasing temperature. Thus, at lower bath temperatures, the thermal conductivity of the liquid EDM would be lower than at higher bath temperatures. A lower thermal conductivity, according to Equation (4.11), the lower the heat transfer coefficient becomes. This may be even more influential in the boundary layer. Since this variation in thermal conductivity was not reported in the research, it was not included in the model.

Another reason that the model and the experimental data may not have matched for the stirred EDM bath could be the inaccuracy of the solid EDM layer on the stainless steel tube. The thickness was measured by pulling the bulkhead out of the apparatus and measuring the solidified EDM on the surface of the tube. Since it was not in the apparatus while the frozen salt was being measured, the solid EDM thickness may not be an accurate representation of the frozen layer.

Using the model, an analysis of the heat transfer resistances involving the stirred EDM bath was performed. Heat transfer resistances appear in Equation (4.23) in the denominator with two resistances for conduction in the steel and frozen salt layers and two resistances for convection on the inside of the steel

tube and the outside of the frozen salt layer. These calculations show which layer provides the largest resistance to heat transfer. The first encountered resistance is within the boundary layer on the outside of the frozen salt, which has a value of 0.102 m-°C/W. According to the model, the frozen EDM layer had the highest resistance range (due to changes of the thickness as a function of bath temperature) of 0.254 m-°C/W to 0.120 m-°C/W. This is followed by the inside boundary layer and the steel layer which had resistances of 0.0532 m-°C/W and 0.0137 m-°C/W, respectively. This shows that the main resistance to heat transfer was the frozen EDM layer due to its low thermal conductivity. Elimination of this layer should result in higher heat flux.

Since there are salt systems that reach higher than the operating temperature of the stirred EDM apparatus, higher heat fluxes could be obtained in future experiments. At 500°C the model predicts a heat flux of 1.53 Btu/in^{2}s using EDM as the heat transfer fluid and water as the test fluid. By extrapolating, the model predicts a heat flux of 4.00 Btu/in^{2}s at 1000°C for the same system. However, the EDM will not operate at 1000°C since it decomposes at 566°C. With other salt systems and more heat provided to them by a different apparatus configuration, these high heat fluxes may be possible. Using a different salt system may have the complication of a solid layer forming on the test piece within the different operating temperature range. Since the steel skin temperature may be below the melting point of that particular salt system. However, with a higher operating temperature range, higher heat fluxes should be achieved.

CHAPTER VI

CONCLUSIONS AND FURTHER WORK

The overall design of the immersion EDM bath resulted in heat fluxes up to 1.645 Btu/in^{2}s at steady state flow of water at 0.435 L/min (18.8 ft/s). The predictive model for both water and EDM baths matched the general trend, but the model over predicted the resultant heat flux for the EDM bath at lower temperatures. A better understanding of the interactions that occur at the liquid-solid interface of the EDM bath is necessary for a more accurate model.

A major issue of the modeling was attempting to find a correlation for the outer heat transfer coefficient. Several models were examined to determine which one would be best suited to model the conditions of heat transfer of the stirred EDM and water baths. These models used parameters specific to the conditions of their experiments, such as placement and design of the impeller, impeller diameter, rotational speed, baffling, and container geometry, none of which matched the specifics of the immersion bath. Thus, an attempt was made to model the outer heat transfer coefficient by assuming flow past a vertical pipe model. This would eliminate the need for geometry and configuration specific modeling. The overall discrepancy between the data and the model was around 11.3% for the stirred water bath and 25.5% for the stirred EDM bath.

There are several reasons why the experimental data and the model did not match. The first is that the model was based on empirical data collected from many years of heat exchanger modeling. Empirical models are based on specific configurations, which may have different efficiencies, and thus may produce different heat flux at similar temperatures and flow rates. In addition to configuration, certain assumptions had to be made about the heat transfer medium. No data was available regarding the variation of thermal conductivity or heat capacity as a function of temperature for both the liquid and frozen salt. These two quantities were assumed constant for the operating range. Also, the actual thickness of the frozen EDM was never measured while the test piece was submerged, which would imply that the frozen salt could have been thicker or non-uniform while immersed. These effects would help to explain why the temperature of the water did not reach the temperatures predicted by the model, thus resulting in a lower experimental heat flux.

With regard to future experimentation, there are some changes that may result in better performance of the stirred immersion bath. The first such change would be a temperature controller, such as a proportional or PID controller. Only manual dials and thermocouples were available to adjust the temperature of the bath, and a controller would eliminate the risk of overshoot and time consumption that is common for a manually controlled system. Another change to the system could be the addition of cartridge heaters that could be lowered into the immersion fluid. The main reason that these should be added to the system is because the kiln apparatus had difficulty going above 485°C when the maximum

operating temperature of the EDM is about 565°C [12]. Not only would the heaters increase the maximum operating temperature, but they could also be used as baffles within the heat transfer fluid. This would be especially important if a different heat transfer fluid was used in future experimentation. EDM was chosen because it does not require safety systems, such as a nitrogen blanket or other inert atmosphere, and because there is little interaction between the salt and the container. Using other transport media may increase the operating temperature of the immersion bath, especially with the addition of cartridge heaters. Higher operating temperatures would increase the thermal gradient across the boundary layers and the steel pipe, resulting in higher heat flux. Some examples of other heat transfer salts could be $NaAlF_4$ or AlF_3, which melt at 775°C and 445°C, respectively [20]. Since their melting temperatures are higher than that of EDM, they should have a higher operating temperature range.

Different test fluids should be used in future experiments since the original intention of the immersion bath was to simulate high heat flux of fuels used in propulsion. The typical temperature range of the test fluid was 17.5°C to 74.3°C, whereas the typical turbine engine can reach up to 625°C [5]. Also, the walls of engine combustion chambers have reached up to 690°C [6]. A pre-heater could warm the test fluid such that heat flux behavior could be observed at higher temperatures. Lower heat flux should be expected in this configuration since the temperature difference would be smaller. Also, different fluids could be used in the apparatus. Test fluids of interest of the USAF would be propulsion fluids such as JP-8, RP-1, Jet A-1, or TS-1, all of which are kerosene based fuels. For

ease of research, single organic species may be tested such as octane, heptane, or decane. These changes would make the liquid immersion heat flux apparatus a more viable experimental system for fuel research.

APPENDIX

APPENDIX A

The following is a Microsoft Visual Basic program written to model the actual heat transfer of the stirred bath liquid solid heat transfer apparatus using both the water bath and the EDM bath [19].

```
'George Doyle III
'Heat Flux Calculator V1.01
    'V1.0 6/03 Capabilities:
        '- Calculates heat flux in metric and english units
        '- Gives final outstream temperature of test fluid
        '- Current test fluids: water
        '- Current heat transfer fluids: EDM
    'V1.01 8/03:
        '- All capabilities of V1.0 and:
        '- Can choose between water and EDM heat transfer fluids
        '- Includes variable properties of EDM and water
    'V1.02 8/22:
        '- Variable Table added
        '- Salt thickness updated
'Variable Table:
    'Variable       Units           Description
    'ID             inches          Inner diameter of tube
    'HtdL           inches          Heated length of tube
    'XArea0         m^2             cross-sectional area of system
    'HXferArea      m^2             Heat transfer area, encloses system
    'InTemp         °C              Temperature at the inlet of system
    'OutTemp        °C              Temperature at the outlet of system
    'BathTemp       °F              Temperature of heat transfer fluid
    'BathTempC      °C              Temperature of heat transfer fluid
                                    in °C
    'volFR          L/min           volumetric flowrate of test fluid
    'Vz             m/s             time averaged fluid velocity
    'ksteel         W/m-K           thermal conductivity of steel tube
    'ksalt          W/m-K           thermal conductivity of frozen salt
    'Cp0            J/kg-K          heat capacity of test fluid
    'Cp1            Btu/lb-°F       heat capacity of heat transfer
                                    fluid
    'Mu0            kg/m-s          viscosity of test fluid
    'Mu1            cP              viscosity of heat transfer fluid
    'k0             W/m-K           thermal conductivity of test fluid
```

```
    'k1             Btu/ft-hr-°F    thermal conductivity of heat
                                    transfer fluid
    'Rho0           kg/m^3          density of test fluid
    'Rho1           lb/ft^3         density of heat transfer fluid
    'Nrpm           rpm             rotational impeller speed
    'ImpD           in              impeller diameter
    'OD             in              outer diameter of test piece
    'thickness      in              thickness of solid EDM layer
    'Re0            -               Reynolds number of test fluid
    'Re1            -               Reynolds number of heat transfer
                                    fluid
    'Pr0            -               Prandtl number of test fluid
    'Pr1            -               Prandtl number of heat transfer
                                    fluid
    'Nu0            -               Nusselt number of test fluid
    'Nu1            -               Nusselt number of heat transfer
                                    fluid
    'h0             W/m^2-K         Test fluid side heat transfer
                                    coefficient
    'h1             W/m^2-K         Heat transfer fluid side heat
                                    transfer coefficient
    'u0             W/m-K           overall heat transfer coefficient
    'i              -               integer for For,Next loop
    'Qit            W               intermediate heat flow in For,Next
                                    loop
    'Qsum           W               Total heat flow
    'QTemp          W               temporary heat flow variable in
                                    For,Next loop
    'deltaZ         m               cross sectional height
    'dummyTemp      °C              dummy temperature variable for
                                    For,Next loop
    'HFdelivered    W/m^2           delivered heat flux
    'HFmetric       W/m^2           absorbed heat flux
    'HFenglish      Btu/in^2-s      absorbed heat flux in English units

Private Enum HTF
    EDM = 0
    water = 1
End Enum

Private Sub form_load()
'Purpose:  to load the combo box with
'          two heat transfer fluids and
'          set its initial value.

    Call cboHTF.Clear
    Call cboHTF.AddItem("EDM")
    Call cboHTF.AddItem("Water")

    cboHTF.ListIndex = fHTF

End Sub

Private Sub cmdCalc_Click()

    'Define variables and parameters
    Dim Nu0 As Single, Nu1 As Single, Pr0 As Single, Pr1 As Single
```

```
Dim Re0 As Single, Re1 As Double, h0 As Double, h1 As Single
Dim k0 As Single, k1 As Single, Cp0 As Single, Cp1 As Single
Dim Rho0 As Single, Rho1 As Single, Mu0 As Single, Mu1 As Single
Dim ID As Single, OD As Single, SaltTh As Single
Dim InTemp As Single, OutTemp As Single, volFR As Single
Dim HtdL As Single, BathTemp As Single, ImpD As Single, Nrpm As
        Single
Dim XArea0 As Single, HXfer As Single, Vz As Single, Pi As Single
Dim ksteel As Single, deltaZ As Single, Qit As Single, Qsum As
        Single
Dim i As Integer, HFmetric As Single, HFenglish As Single,
        dummyTemp As Single
Dim ksalt As Single, thickness As Single, QTemp As Single

'Input Variables
ID = Val(txtID.Text) 'in
HtdL = Val(txtHtdL.Text) 'in
InTemp = Val(txtInTemp.Text) '°C
volFR = Val(txtVolFR.Text) 'L/min
ksteel = 16.297 'W/mK
ksalt = 2.1 'W/mK

'Define test fluid parameters
Cp0 = 4186.8 'J/kgK
'From a fit of data from McCabe, Smith and Harriot for water:
'Rho0 = -4E-08x4 + 2E-05x3 - 0.0057x2 - 0.0088x + 1000.5
Rho0 = -0.00000004 * (InTemp) ^ 4 + 0.00002 * InTemp ^ 3 - 0.0057 *
        InTemp ^ 2 - 0.0088 * InTemp + 1000.5 'kg/m3
'From a fit of data from McCabe, Smith and Harriott for water:
'Mu0 = -7E-14x5 + 4E-11x4 - 8E-09x3 + 8E-07x2 - 5E-05x + 0.0017
Mu0 = -0.00000000000007 * InTemp ^ 5 + 0.00000000004 * InTemp ^ 4 -
        0.000000008 * InTemp ^ 3 + 0.0000008 * InTemp ^ 2 - 0.00005
        * InTemp + 0.0017 'kg/ms
'From a fit of data from McCabe, Smith and Harriot for water:
'k0 = 3E-08x3 - 1E-05x2 + 0.0025x + 0.5533
k0 = 0.00000003 * InTemp ^ 3 - 0.00001 * InTemp ^ 2 + 0.0025 *
        InTemp + 0.5533 'W/mK

'Calculate inner heat transfer coefficient
Pi = 3.14159265358979
XArea0 = Pi * (ID * 2.54 / 100) ^ 2 * 0.25 'm^2
HXferArea = Pi * (ID * 2.54 * 0.01) * (HtdL * 2.54 / 100) 'm^2
Vz = volFR / 1000 / 60 / XArea0 'm/s
'Calculate Dimensionless Variables
Re0 = (ID * 2.54 / 100) * Vz * Rho0 / Mu0
Pr0 = Cp0 * Mu0 / k0
Nu0 = 0.023 * (Re0 ^ 0.8) * (Pr0 ^ (1 / 3))
'Calculate coefficient
h0 = Nu0 * k0 / (ID * 2.54 / 100) 'W/m2K

'Calculate outer heat transfer coefficient
BathTemp = Val(txtBathTemp.Text) '°F
BathTempC = (Val(txtBathTemp.Text) - 32) * 5 / 9 '°C
Nrpm = Val(txtNrpm.Text)
ImpD = 3.825 'inches
OD = Val(txtOD.Text) 'inches
```

```
'define parameters for heat transfer fluid
If cboHTF.Text = "EDM" Then
    'Calculate Parameters for salt bath:
    Rho1 = 129 - 0.0000096 * (BathTemp) ^ 2 'lb/ft3
    Mu1 = (Exp(-1.404 + 1747.7 / (BathTemp + 116.8))) * 2.4191
        'lb/fthr
    k1 = 0.31 'Btu/fthr°F
    Cp1 = 0.38 'Btu/lb°F
    'Calculate Salt Thickness:
    'y = 472.72*(T)^-1.7639 is the equation given by Excel, where x
        is the bath
    'temperature in degrees Celsius and y is the thickness in
        inches.
    thickness = 472.72 * (BathTempC) ^ (-1.7639) 'inches
    'Calculate Dimensionless Parameters for salt bath
    Re1 = (Nrpm * 60 * Pi * (2 / 12 * 2)) * (OD + 2 * thickness) /
        12 * Rho1 / Mu1
    Pr1 = Cp1 * Mu1 / k1
    Nu1 = 0.3 + (0.62 * Re1 ^ 0.5 * Pr1 ^ (1 / 3)) * ((1 + (Re1 /
        282000) ^ (5 / 8)) ^ (4 / 5)) / (1 + (0.4 / Pr1)) ^ 0.25
    'calculate heat transfer coefficient for salt bath
    h1 = Nu1 * k1 / ((OD + thickness * 2) / 12) * 5.6782 'W/m2K
    'Calculate Overall Heat transfer coefficient for salt bath
    u0 = 1 / (1 / (ID / 200 * 2.54 * h0) + (Log(OD / ID)) / ksteel
        + (Log((OD + 2 * thickness) / OD)) / ksalt + 1 / ((OD + 2 *
        thickness) / 200 * 2.54 * h1)) / (ID * 2.54 / 200)
ElseIf cboHTF.Text = "Water" Then
    'Calculate Parameters for water bath
    'From McCabe, Smith and Harriott y = 7E-08x3 - 9E-05x2 +
        0.0035x + 62.473:
    Rho1 = (0.00000007 * BathTemp ^ 3) - (0.00009 * BathTemp ^ 2) +
        (0.0035 * BathTemp) + 62.473 'lb/ft3
    Cp1 = 1.05 'Btu/lb°F
    Mu1 = 1.7628 * Exp(-0.0088 * BathTemp) 'cP
    k1 = 0.043 * Log(BathTemp) + 0.1643 'Btu/fth°F
    'Calculate Dimensionless Parameters for water bath
    Re1 = (Nrpm * 60 * Pi * (2 / 12 * 2)) * (OD / 12) * Rho1 / Mu1
    Pr1 = Cp1 * Mu1 / k1
    Nu1 = 0.3 + (0.62 * Re1 ^ 0.5 * Pr1 ^ (1 / 3)) * ((1 + (Re1 /
        282000) ^ (5 / 8)) ^ (4 / 5)) / (1 + (0.4 / Pr1)) ^ 0.25
    'Calculate the heat transfer coefficient for the water bath
    h1 = Nu1 * k1 / (OD / 12) * 5.6782 'W/m2K
    'Calculate Overall Heat transfer coefficient
    u0 = 1 / (1 / (ID / 200 * 2.54 * h0) + (Log(OD / ID)) / ksteel
        + 1 / (OD / 200 * 2.54 * h1)) / (ID * 2.54 / 200)
End If

'Compute each finite volume to find the final temperature and total
        heat flux
i = 1
deltaZ = Val(txtHtdL.Text) / 100 * 2.54 / 100
Qsum = 0
dummyTemp = InTemp 'element inlet temp

For i = 1 To 100
    Qit = 2 * Pi * deltaZ * u0 * (ID * 2.54 / 200) * (BathTempC -
        dummyTemp)
```

```
        Qsum = Qsum + Qit
        OutTemp = Qit / (Cp0 * Rho0 * volFR / 60 / 1000) + dummyTemp
        dummyTemp = OutTemp
    Next i

    'output the final results
    txtOutTemp.Text = OutTemp
    txtHeat.Text = Qsum
    HFmetric = (OutTemp - InTemp) * volFR * Rho0 / 1000 / 60 * Cp0 /
            (Pi * (HtdL * 2.54 / 100) * (0.05 * 2.54 / 100)) 'W/m2
    txtHFmetric.Text = HFmetric
    HFenglish = HFmetric / 1635344.64 'Btu/in2s
    txtHFenglish.Text = HFenglish
End Sub

Private Sub cmdExit_Click()
    Unload frmHFCalc
End Sub

Private Sub cmdPrint_Click()
    PrintForm
End Sub
```

APPENDIX B

Table B.1 shows the fluid characteristics of water and EDM at proper temperatures for the experiments.

Table B.1: Properties of Heat Transfer Fluids:

Property	Water	EDM
Fluid Type	Newtonian	Newtonian
Viscosity (cP)	1.00 @ 20°C	1.65 @ 427°C
Thermal Conductivity (solid) (W/mK)	2.25 @ 0°C	2.1 @ 20°C
Thermal Conductivity (liquid) (W/mK)	0.597 @ 20°C	0.537 @ 427°C
Density (kg/m3)	999 @ 20°C	1970 @ 427°C
Heat Capacity (J/kg°C)	4820 @ 20°C	884 @ 427°C

REFERENCES CITED

1. Gray, Dale M. "Amateur Rocketry Takes Flight." http://www.spacepolicty.org/page_dg0400.html. 2003.

2. "The New Mexico Museum of Space History – Inductee – James H. Wyld." http://www.spacefame.org/wyld.html. 2003.

3. "F-1 Engine Fact Sheet." Saturn V News Reference. August 1967.

4. Godwin, Robert. X-15: The NASA Mission Reports. Burlington, ON: Apogee Books. 2000.

5. "Technical Review: Aviation Fuels." San Ramon, CA: Chevron Products Co. 2000.

6. Wagner, W. R., and Shoji, J. M. "Advanced Regenerative Cooling Techniques for Future Space Transportation Systems." AIAA Paper 75-1247. Sep. 1975.

7. Fleig, Oliver. "Cooling of the Rocket Engine." http://www.visionengineer.com/aero/cooling.shtml. 2003.

8. Weigel, N., D. Wiedmann, A. Frölich. "Critical Topics for Rocket Engine Thrust Chamber Life Predition." CNES-AAAF-ESA Conference. Liége, Belgium. Dec 2002.

9. Wills, Richard W. Propulsion Directorate, Air Force Research Laboratories, Wright Patterson Air Force Base. Personal Communication. 2003.

10. Palaszewski, Bryan A. "Metallized Gelled Propellants: Heat Transfer of a Rocket Engine Fueled by Oxygen/RP-1/Aluminum Was Measured by a Calorimeter." http://www.grc.nasa.gov/WWW/RT1997/5000/5830palaszewski2.htm. April 1998.

11. Dickens, K. W., D. L. Linne, N. J. Georgiadis. "Experiment and Modeling of a Rocket Engine Heat Flux Environment for Materials Testing." AIAA 2003-0283. 41st Aerosace Sciences Meeting & Exhibit. 6-9 Jan 2003, Reno, NV.

12. Guyer, Eric C., David L. Brownell. Handbook of Applied Thermal Design. Philadelphia, PA: Taylor & Francis. 1999.

13. Tester, Jefferson W., Michael Modell. Thermodynamics and Its Applications. 3rd Ed. Upper Saddle River, NJ: Prentice Hall PTR. 1997.

14. McCabe, Warren L., Julian C. Smith, Peter Harriott. Unit Operations of Chemical Engineering. 6th Ed. Boston: McGraw-Hill. 2001.

15. Bird, R. Byron, Warren E. Stewart, Edwin N. Lightfoot. Transport Phenomena. New York: John Wiley & Sons. 1960.

16. Churchill, S. W., M. Bernstein. "A Correlating Equation for Forced Convection From Gases and Liquids to a Circular Cylinder in Crossflow." Transactions of ASME: Journal of Heat Transfer. Vol 99 May 1977.

17. Oldshue, James Y. Fluid Mixing Technology. New York: McGraw Hill. 1983.

18. Maple Release V. Waterloo Maple, Inc. 1981-1997.

19. Microsoft Visual Basic 6.0. Microsoft Corporation 1987-1998.

20. Lovering, David G., Robert J. Gale. Molten Salt Techniques. Vol 1. New York: Plenum Publishing. 1983.